


 CrossMark
click for updates

 Cite this: *CrystEngComm*, 2015, 17, 9070

Structures and trends of one-dimensional halide-bridged polymers of five-coordinate cadmium(II) and mercury(II) with benzopyridine and -pyrazine-type N-donor ligands†

C. Slabbert and M. Rademeyer*

Cadmium and mercury dihalides were reacted with benzopyridine- and benzopyrazine-type N-donor ligands as Lewis bases. The solid-state structures of 13 novel reaction products were studied by X-ray diffraction. Eleven of the structures can be classified as one-dimensional halide-bridged polymers of composition $[M(\mu-X)_2(L)]_{\infty}$, in which the metal ion displays a coordination number of five, while the remaining two structures exhibit one-dimensional dimers that are linked by long, semi-coordinate $M-X \cdots M-X$ interactions to form pseudo-halide-bridged polymers. Four of the structures contain Cd^{2+} as the metal ion, while the remaining nine have Hg^{2+} as the metal ion. Although all the halide-bridged polymers show a coordination number of five, two different metal cation geometries are displayed. A detailed comparison of all structural results, which includes related compounds from the literature and allows for the study of the effect of an increase in the width of the N-donor ligand on the halide-bridged chain geometries and other structural features, concludes the discussion.

 Received 8th July 2015,
Accepted 17th October 2015

DOI: 10.1039/c5ce01333j

www.rsc.org/crystengcomm

Introduction

The term “Crystal Engineering” has matured from a fancy catch phrase to a widely used verb, the application of which refers to the study and understanding of intermolecular interactions and concomitant packing modes in order to enable the user to exploit this knowledge to construct premeditated solid-state structures from appropriate precursors.^{1–4}

One of the most fascinating and most extensively studied research areas that fall under the interdisciplinary umbrella of crystal engineering is that of coordination polymers.^{4,5} This is deservedly so, since not only are the resulting structures aesthetically mesmerizing, but also the utilisation of these crystalline solids has its footing in materials science, medicinal and environmental chemistry, and nanotechnology.⁵

Even though a fair number of potential applications ascribed to coordination polymers can be extrapolated to halide-bridged polymers of metal cations with organic donor ligands, and although the halide-bridged polymeric scaffold has earned its synthon status,⁶ this subdivision is structurally uncharted. The study of halide-bridged polymers of divalent

d^{10} metal cations with N-donor ligands is by no means a solitary endeavour and recent efforts by Englert and coworkers^{6–9} and Mahmoudi and Morsali¹⁰ have contributed greatly to the enrichment of our current understanding of these compounds through excellent research papers and the addition of numerous structures to the structural data bank. Comprehensive review articles are also available.^{11–13} The work presented in this article aims to build on this knowledge. The focus of both Englert *et al.*^{6,8,9} and Mahmoudi and Morsali¹⁰ was on the effect of electronically modified pyridine/pyrazine-derived N-donor ligands on the structural type presented by the coordinated halide-bridged chain. As a natural progression, in this paper, we investigate the role of the electronic nature and spatial extension of the organic ligand in the one-dimensional (1D) halide-bridged chain by taking benzo-substituted pyridine/pyrazine-type organic ligands of different widths into consideration. We address the questions of the extent to which the width of the coordinating N-donor organic ligand can therefore be increased without disrupting the chain integrity, and if this, as well as the specific bridging halide ion, affects the coordination geometry adopted by the metal cation.

The current study reports structures of the expected formal composition $[MX_2L_2]_{\infty}$, where M represents a divalent group 12 metal cation with an nd^{10} electronic configuration, X stands for a halide ligand, Cl^- , Br^- or I^- , L indicates a mono- or ditopic N-donor organic ligand, which is either

Department of Chemistry, University of Pretoria, cnr Lynnwood Road & Roper Street, Hatfield, Pretoria 0002, South Africa. E-mail: melanie.rademeyer@up.ac.za

† Electronic supplementary information (ESI) available: CCDC 1409084–1409096. For ESI and crystallographic data in CIF or other electronic format see DOI: 10.1039/c5ce01333j

acridine (acr)/phenazine (phe) or quinoline (quin), and the infinity sign represents polymeric extension in one dimension. No neutral halide-bridged one-dimensional polymers containing either of the target metal cations with the related molecule quinoxaline as the monotopic N-donor ligand were found in this study, or in the literature. The organic ligands of interest are illustrated schematically in Table 1. Zero-dimensional mononuclear complexes and anionic perhalometallates encountered will be reported in sister articles, while the present article exclusively focuses on neutral halide-bridged polymers observed in this study. Here, we report eleven novel 1D halide-bridged polymers and two novel dimeric systems, as organised in Table 1.

The abbreviation $[M(\mu-X)_2(L)]_\infty$ will be employed to label the halide-bridged polymers, with M indicating the metal ion, X the halide anion and L = acr, phe or quin. Table 1 also includes related structures EYETOS,¹⁴ EYERUW¹⁴ and EYSEH,¹⁴ which are available in the literature and will be included in the structural comparison.

The effort leans toward correlating the obtained structural types with the variable components, M, X and L, to be able to formalise trends identifiable within the current set of structures as well as related structures from the literature. Eleven of the thirteen compounds comprise one-dimensional halide-bridged polymers of five-coordinate divalent metal cations coordinated to one N-donor ligand per metal node. A survey of the Cambridge Structural Database (CSD)¹⁵ (version 5.36 including the February 2015 update) was conducted to determine the frequency of occurrence of this type of halide-bridged polymer. The search fragment comprised any divalent group 12 metal centre, restrained to be five-coordinate, coordinated to any four halide ligands *via* one polymeric bond and three bonds defined to include any type of bond and one nitrogen atom. The donating three-coordinate nitrogen atom was connected to the metal centre *via* any type of bond and further bonded to two R groups *via* any bond, indicating substitution with any two atoms on the nitrogen atom. Default parameters were used in defining the bond types. The resulting hits were sifted manually and revealed that one-dimensional halide-bridged polymers of five-coordinate divalent d¹⁰ metal cations coordinated by only one N-donor ligand are the exception rather than the rule, with only 26

hits, compared to 170 hits when the divalent group 12 metal centre is six-coordinated to four halide ligands and two N-donor atoms (bond length criteria and nitrogen substitution were defined in the same way as in the previous search).

Results and discussion

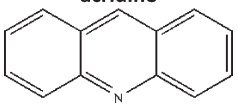
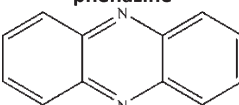
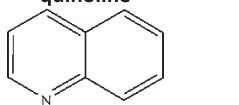
Thirteen novel crystal structures were determined, as listed in Table 1. Eleven structures (1–5 and 7–12) can be classified as one-dimensional halide-bridged polymers in which the metal ion displays a coordination number of five, while the remaining two structures (6 and 13) exhibit one-dimensional dimers that are linked by long, semi-coordinate M–X⋯M–X interactions to form pseudo-halide-bridged polymers. Four of the structures contain Cd²⁺ as the metal ion, while the remaining nine have Hg²⁺ as the metal ion. A detailed comparison of all results, which include related compounds from the literature, concludes the discussion.

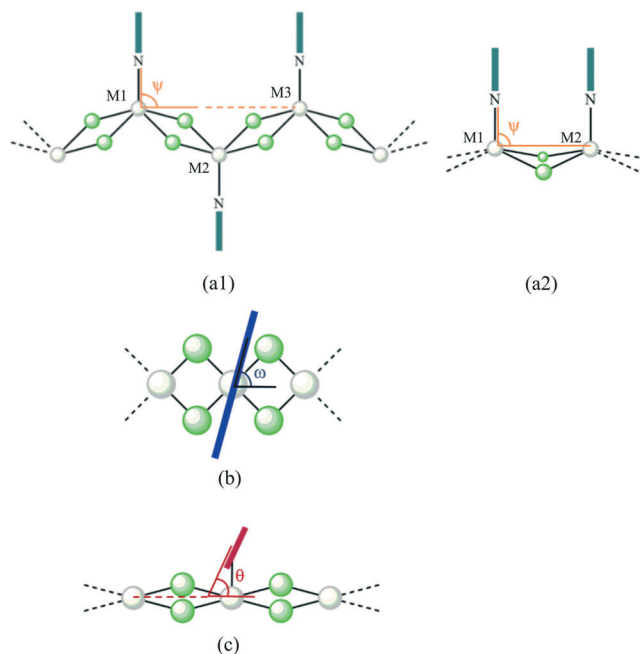
Due to the presence of metal halide-bridged chains or metal halide-bridged pseudo-chains, in all the structures, in this contribution, the descriptors ψ , ω and θ , introduced by Hu, Li & Englert⁶ to describe different orientations that coordinated pyridine-type ligands may adopt relative to a halide-bridged polymeric chain, will be employed. These descriptors, adapted for the present structures, are presented schematically in Scheme 1, and will be used throughout the text as a classification aid.

ψ indicates the angle between the M–N line, which refers to the bond between the metal centre and the organic ligand donor atom, and the M⋯M vector. In the case where the metal ions in the metal halide-bridged polymer are not co-linear, the M⋯M vector is taken as the vector between alternating metal ions, as illustrated in Scheme 1, a1. However, when the metal ions are co-linear, the M⋯M vector is defined between neighbouring metals, as shown in Scheme 1, a2. Neighbouring metal atoms will be labelled generically as M(1) and M(2), while M(1) and M(3) are the next nearest neighbours, as shown in Scheme 1.

θ measures the tilt angle of the mean ring plane relative to the same M⋯M vector, while ω is a dihedral angle, which measures the rotation of the mean ring plane around the M–N bond against the M⋯M vector.

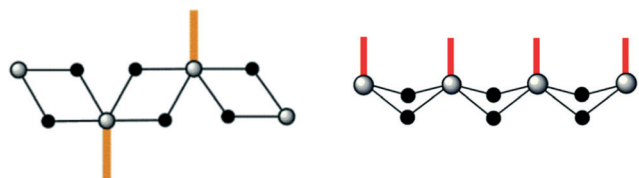
Table 1 Reported structures with allocated numbering scheme

M ²⁺	μ -Halide	acridine			phenazine			quinoline		
										
Cd ²⁺	Cl [−]	$[Cd(\mu-Cl)_2(acr)]_\infty$	1	$[Cd(\mu-Cl)_2(phe)]_\infty$	7	$[Cd(\mu-Cl)_2(quin)]_\infty$, EYETOS ¹⁴				
	Br [−]	$[Cd(\mu-Br)_2(acr)]_\infty$	2			$[Cd(\mu-Br)_2(quin)]_\infty$, EYERUW ¹⁴				
	I [−]	$[Cd(\mu-I)_2(acr)]_\infty$	3			CdL ₂ quin ₂ , EYSEH ¹⁴				
Hg ²⁺	Cl [−]	$[Hg(\mu-Cl)_2(acr)]_\infty$	4	$[Hg(\mu-Cl)_2(phe)]_\infty$	8	$[Hg(\mu-Cl)_2(quin)]_\infty$			11	
	Br [−]	$[Hg(\mu-Br)_2(acr)]_\infty$	5	$[Hg(\mu-Br)_2(phe)]_\infty$	9	$[Hg(\mu-Br)_2(quin)]_\infty$			12	
				$[Hg_2(\mu-Br)_4(\mu-phe)]_\infty$	10					
	I [−]	$[Hg_2(\mu-I)_2I_2(acr)_2]$	6			$[Hg_2(\mu-I)_2I_2(quin)_2]$			13	



Scheme 1 Schematic representation of the descriptors ψ (a1 and a2), ω (b) and θ (c) indicating the orientation of the organic N-donor ligand relative to the one-dimensional halide-bridged chains of the type $[M(\mu-X)_2]$, where $M = \text{Cd}^{2+}$, Hg^{2+} and $X = \text{Cl}^-$, Br^- or I^- . The diagrams were adapted for the reported systems from Hu *et al.*⁶ The light grey spheres represent the metal cations, the light green spheres the bridging halide ligands and the thick turquoise, blue and maroon lines the N-donor organic ligands.

Even though structures 1–5 and 7–12 all show a coordination number of five, two different types of metal cation geometries are displayed. The metal centres in structures 1–5 as well as 11 and 12 are all trigonal bipyramidal, while the metal centres in 8–10 all approach a square pyramidal geometry. When compounds 6 and 13 are considered as isolated dimers, the metal centres are of tetrahedral geometry, however, when the dimers are viewed as constituents of pseudo-one-dimensional chains, the geometry of the metal centre can be taken as distorted square pyramidal, thus again a five-coordinate system. The overriding halide-bridged chain motif displayed is a zigzag ribbon (Scheme 2, left), while only compound 10 exhibited a scalloped-ribbon motif (Scheme 2, right). In the following section, the structures are divided into sub-categories according to the space group setting, with structures 1–5 and 7 crystallising in the monoclinic space



Scheme 2 Schematic representation of a zigzag ribbon motif (left) and scalloped-ribbon motif (right) in which the grey spheres represent the metal cations, the black spheres the bridging halide ligands and the thick orange/vermillion lines the coordinated N-donor ligands.

group $C2/c$, and structures 6 and 8–13 all crystallising in the triclinic space group $P\bar{1}$. This categorization also groups together similar structures. Crystallographic data for all the structures are listed in Table 2.

$[\text{Cd}(\mu-X)_2(\text{acr})]_\infty$ (1–3), $[\text{Cd}(\mu-\text{Cl})_2(\text{phe})]_\infty$ (7) and $[\text{Hg}(\mu-X)_2(\text{acr})]_\infty$ (4 and 5)

Compounds 1–5 and 7 are isostructural and crystallise in the monoclinic space group $C2/c$. All these compounds, except structure 2, were prepared with an organic ligand-to-metal halide salt ratio of 1:1, and this ratio is also reflected in the structure obtained. Even though an organic ligand-to-metal halide salt ratio of 2:1 was employed in the synthesis of 2, the structure obtained also displays a ratio of 1:1, which may be attributed to the stability of this specific type of complex. The asymmetric units of 1–3 all consist of a Cd^{2+} ion coordinated to one halide ligand and one half of an acridine ligand *via* the nitrogen atom as an L-type donor atom, with the halide ligands ranging from chloride to bromide to iodide. The asymmetric unit of 7 also consists of a Cd^{2+} ion coordinated to one chloride ligand, but here the coordinating ligand is one half of a phenazine ligand which coordinates *via* one nitrogen atom only. The asymmetric units of 4 and 5 differ from those of 1–3 and 7, in that the metal centres are Hg^{2+} ions, again with acridine as the organic N-donor ligand, and chloride and bromide as the halide ligands, respectively. The asymmetric unit of each compound is given in Fig. 1 (left). In all the structures, the M^{2+} cations and N(1), C(7) (compounds 1–5) or N(2) (compound 7) and H(7) atoms occupy special positions at $(0, x, \frac{1}{4})$, lying on a 2-fold rotation axis with direction $[0, 1, 0]$ at $(0, y, \frac{1}{4})$, which generates the full repeat unit, as illustrated in Fig. 1 (right). Four asymmetric units comprise each unit cell.

Structures 1–5 and 7 all form one-dimensional halide-bridged polymers composed of five-coordinate M^{2+} metal centres, connected by two bridging halide ligands as edge-sharing trigonal bipyramids, and terminal organic ligands, as illustrated in Fig. 2.

The halide-bridged chain adopts a zigzag ribbon motif, as schematically presented in Scheme 2, with the organic N-donor ligands alternating between the ‘above’ and ‘below’ positions on successive metal centres in the halide-bridged chain when viewed perpendicular to the direction of chain propagation, as illustrated in Fig. 2 (right). The trigonal base plane in all of the compounds consists of two halide ligands and one nitrogen atom of the organic donor ligand coordinated to the metal centre. The apical positions of the trigonal bipyramids are coordinated by two halide ligands, as illustrated in Fig. 2 (left). The acridine or phenazine ligands can be considered planar. Selected geometric parameters related to the polymer chain geometry, including ψ , θ and ω , are listed in Table 3. In all cases, the polymer chain propagates along the direction of the shortest lattice parameter, the c -axis, with the distance between the alternating metal centres also equal to the c cell spacing. The b and c unit cell

Table 2 Crystallographic parameters and refinement results for compounds 1–13

Structure	1	2	3
Abbreviation	[Cd(μ -Cl) ₂ (acr)] _∞	[Cd(μ -Br) ₂ (acr)] _∞	[Cd(μ -I) ₂ (acr)] _∞
Empirical formula	C ₁₃ H ₉ NCdCl ₂	C ₁₃ H ₉ NCdBr ₂	C ₁₃ H ₉ NCdI ₂
Formula weight (g mol ⁻¹)	362.51	451.43	545.41
Temperature	293(2) K	293(2) K	293(2) K
Wavelength	0.71073 Å	0.71073 Å	0.71073 Å
Crystal system	Monoclinic	Monoclinic	Monoclinic
Space group	<i>C2/c</i>	<i>C2/c</i>	<i>C2/c</i>
Unit cell dimensions	<i>a</i> = 18.041(2) Å <i>b</i> = 10.0013(13) Å <i>c</i> = 7.0529(9) Å β = 111.642(5)°	<i>a</i> = 18.1586(8) Å <i>b</i> = 10.3322(5) Å <i>c</i> = 7.2771(4) Å β = 110.45(3)°	<i>a</i> = 17.7013(8) Å <i>b</i> = 10.7920(5) Å <i>c</i> = 7.6053(3) Å β = 107.355(2)°
Volume	1182.9(3) Å ³	1279.3(3) Å ³	1386.72(11) Å ³
Z	4	4	4
Density (calculated)	2.036 Mg m ⁻³	2.344 Mg m ⁻³	2.612 Mg m ⁻³
Absorption coefficient	2.269 mm ⁻¹	7.928 mm ⁻¹	6.004 mm ⁻¹
<i>F</i> (000)	704	848	992
Crystal size	0.122 × 0.081 × 0.032 mm ³	0.10 × 0.07 × 0.03 mm ³	0.126 × 0.108 × 0.105 mm ³
Theta range for data collection	2.371 to 33.047°	2.306 to 27.487°	2.239 to 34.977°
Reflections collected	22 730	6850	40 004
Independent reflections	2229 [<i>R</i> _(int) = 0.0978]	1471 [<i>R</i> _(int) = 0.0415]	3040 [<i>R</i> _(int) = 0.0726]
Completeness to θ	99.9%	99.9%	100.0%
Max. and min. transmission	0.7465 and 0.6399	0.926 and 0.661	0.7469 and 0.5385
Data/restraints/parameters	2229/0/79	1471/0/68	3040/0/79
Goodness-of-fit on <i>F</i> ²	1.108	1.070	1.074
Final <i>R</i> indices [<i>I</i> > 2 σ (<i>I</i>)]	<i>R</i> ₁ = 0.0822, <i>wR</i> ₂ = 0.2544	<i>R</i> ₁ = 0.0293, <i>wR</i> ₂ = 0.0713	<i>R</i> ₁ = 0.0276, <i>wR</i> ₂ = 0.0642
<i>R</i> indices (all data)	<i>R</i> ₁ = 0.0939, <i>wR</i> ₂ = 0.2627	<i>R</i> ₁ = 0.0534, <i>wR</i> ₂ = 0.0804	<i>R</i> ₁ = 0.0379, <i>wR</i> ₂ = 0.0683
Largest diff. peak and hole	8.077 and -2.027 e Å ⁻³	0.851 and -1.509 e Å ⁻³	1.998 and -0.698 e Å ⁻³
Structure	4	5	6
Abbreviation	[Hg(μ -Cl) ₂ (acr)] _∞	[Hg(μ -Br) ₂ (acr)] _∞	[Hg ₂ (μ -I) ₂ I ₂ (acr) ₂]
Empirical formula	C ₁₃ H ₉ NHgCl ₂	C ₁₃ H ₉ NHgBr ₂	C ₂₆ H ₁₈ N ₂ Hg ₂ I ₄
Formula weight (g mol ⁻¹)	450.70	539.62	1267.20
Temperature	293(2) K	293(2) K	293(2) K
Wavelength	0.71073 Å	0.71073 Å	0.71073 Å
Crystal system	Monoclinic	Monoclinic	Triclinic
Space group	<i>C2/c</i>	<i>C2/c</i>	<i>P1</i>
Unit cell dimensions	<i>a</i> = 17.8278(6) Å <i>b</i> = 10.0406(4) Å <i>c</i> = 7.1913(2) Å β = 111.792(2)°	<i>a</i> = 17.9548(13) Å <i>b</i> = 10.3152(8) Å <i>c</i> = 7.4205(5) Å β = 110.814(2)°	<i>a</i> = 8.1694(4) Å <i>b</i> = 9.1306(4) Å <i>c</i> = 9.9609(5) Å α = 84.347(2)° β = 70.877(2)° γ = 77.262(2)°
Volume	1195.26(7) Å ³	1284.64(16) Å ³	684.44(6) Å ³
Z	4	4	1
Density (calculated)	2.505 Mg m ⁻³	2.790 Mg m ⁻³	3.074 Mg m ⁻³
Absorption coefficient	13.296 mm ⁻¹	18.176 mm ⁻¹	15.731 mm ⁻¹
<i>F</i> (000)	832	976	560
Crystal size	0.10 × 0.07 × 0.02 mm ³	0.320 × 0.040 × 0.040 mm ³	0.360 × 0.148 × 0.068 mm ³
Theta range for data collection	2.372 to 32.036°	2.318 to 30.501°	2.165 to 26.371°
Reflections collected	6508	7569	19 502
Independent reflections	2075 [<i>R</i> _(int) = 0.0981]	1961 [<i>R</i> _(int) = 0.0315]	2804 [<i>R</i> _(int) = 0.0444]
Completeness to θ	100.0%	100.0%	99.9%
Max. and min. transmission	0.516 and 0.357	0.7477 and 0.5147	0.7481 and 0.3750
Data/restraints/parameters	2075/0/68	1961/22/79	2804/0/154
Goodness-of-fit on <i>F</i> ²	1.020	0.983	1.207
Final <i>R</i> indices [<i>I</i> > 2 σ (<i>I</i>)]	<i>R</i> ₁ = 0.0745, <i>wR</i> ₂ = 0.1979	<i>R</i> ₁ = 0.0250, <i>wR</i> ₂ = 0.0524	<i>R</i> ₁ = 0.0256, <i>wR</i> ₂ = 0.0677
<i>R</i> indices (all data)	<i>R</i> ₁ = 0.0869, <i>wR</i> ₂ = 0.2099	<i>R</i> ₁ = 0.0387, <i>wR</i> ₂ = 0.0561	<i>R</i> ₁ = 0.0257, <i>wR</i> ₂ = 0.0678
Largest diff. peak and hole	11.686 and -5.029 e Å ⁻³	1.363 and -0.468 e Å ⁻³	2.877 and -0.835 e Å ⁻³
Structure	7	8	9
Abbreviation	[Cd(μ -Cl) ₂ (phe)] _∞	[Hg(μ -Cl) ₂ (phe)] _∞	[Hg(μ -Br) ₂ (phe)] _∞
Empirical formula	C ₁₂ H ₈ N ₂ CdCl ₂	C ₂₄ H ₁₆ N ₄ Hg ₂ Cl ₄	C ₁₂ H ₈ N ₂ HgBr ₂
Formula weight (g mol ⁻¹)	363.50	903.39	540.61
Temperature	293(2) K	293(2) K	293(2) K
Wavelength	0.71073 Å	0.7107 Å	0.71073 Å
Crystal system	Monoclinic	Triclinic	Triclinic

Table 2 (continued)

Structure	7	8	9
Space group	<i>C2/c</i>	<i>P</i> $\bar{1}$	<i>P</i> $\bar{1}$
Unit cell dimensions	<i>a</i> = 16.6766(9) Å <i>b</i> = 10.0104(5) Å <i>c</i> = 7.0588(3) Å β = 96.055(2)°	<i>a</i> = 7.7038(2) Å <i>b</i> = 9.0194(2) Å <i>c</i> = 9.5803(3) Å α = 64.986(2)° β = 80.681(2)° γ = 82.477(2)°	<i>a</i> = 8.0543(4) Å <i>b</i> = 9.3336(5) Å <i>c</i> = 9.7594(5) Å α = 64.112(2)° β = 75.888(2)° γ = 83.030(2)°
Volume	1171.82(10) Å ³	593.82(3) Å ³	640.03(6) Å ³
<i>Z</i>	4	1	2
Density (calculated)	2.060 Mg m ⁻³	2.526 Mg m ⁻³	2.805 Mg m ⁻³
Absorption coefficient	2.293 mm ⁻¹	13.384 mm ⁻¹	18.244 mm ⁻¹
<i>F</i> (000)	704	416	488
Crystal size	0.153 × 0.095 × 0.017 mm ³	0.23 × 0.12 × 0.02 mm ³	0.64 × 0.13 × 0.032 mm ³
Theta range for data collection	2.376 to 27.989°	2.363 to 29.980°	2.375 to 26.369°
Reflections collected	14 520	8513	14 560
Independent reflections	1415 [<i>R</i> _(int) = 0.0540]	3435 [<i>R</i> _(int) = 0.0513]	2614 [<i>R</i> _(int) = 0.0596]
Completeness to θ	100.0%	100.0%	100.0%
Max. and min. transmission	0.7456 and 0.6387	0.908 and 0.689	0.7474 and 0.3095
Data/restraints/parameters	1415/0/79	3435/0/154	2614/0/154
Goodness-of-fit on <i>F</i> ²	1.071	1.095	1.063
Final <i>R</i> indices [<i>I</i> > 2 σ (<i>I</i>)]	<i>R</i> ₁ = 0.0295, <i>wR</i> ₂ = 0.0686	<i>R</i> ₁ = 0.0325, <i>wR</i> ₂ = 0.0860	<i>R</i> ₁ = 0.0787, <i>wR</i> ₂ = 0.2030
<i>R</i> indices (all data)	<i>R</i> ₁ = 0.0368, <i>wR</i> ₂ = 0.0715	<i>R</i> ₁ = 0.0488, <i>wR</i> ₂ = 0.1129	<i>R</i> ₁ = 0.0923, <i>wR</i> ₂ = 0.2177
Largest diff. peak and hole	2.047 and -0.686 e Å ⁻³	2.668 and -2.098 e Å ⁻³	9.605 and -4.349 e Å ⁻³
Structure	10	11	
Abbreviation	[Hg ₂ (μ -Br) ₄ (μ -phe)] _∞	[Hg(μ -Cl) ₂ (quin)] _∞	
Empirical formula	C ₁₂ H ₈ N ₄ Hg ₂ Br ₂	C ₉ H ₇ NHgCl ₂	
Formula weight (g mol ⁻¹)	901.02	400.65	
Temperature	293(2) K	293(2) K	
Wavelength	0.71073 Å	0.71073 Å	
Crystal system	Triclinic	Triclinic	
Space group	<i>P</i> $\bar{1}$	<i>P</i> $\bar{1}$	
Unit cell dimensions	<i>a</i> = 4.0824(2) Å <i>b</i> = 9.6723(5) Å <i>c</i> = 11.1027(5) Å α = 71.406(2)° β = 80.156(2)° γ = 78.525(2)°	<i>a</i> = 7.3885(4) Å <i>b</i> = 7.6432(5) Å <i>c</i> = 9.6655(7) Å α = 68.076(2)° β = 87.897(2)° γ = 88.821(2)°	
Volume	404.48(3) Å ³	506.00(6) Å ³	
<i>Z</i>	1	2	
Density (calculated)	3.699 Mg m ⁻³	2.630 Mg m ⁻³	
Absorption coefficient	28.823 mm ⁻¹	15.685 mm ⁻¹	
<i>F</i> (000)	394	364	
Crystal size	0.324 × 0.102 × 0.020 mm ³	0.323 × 0.094 × 0.089 mm ³	
Theta range for data collection	1.948 to 30.505°	2.759 to 28.281°	
Reflections collected	17 111	2500	
Independent reflections	2457 [<i>R</i> _(int) = 0.0569]	2500 [<i>R</i> _(int) = 0]	
Completeness to θ	99.9%	99.9%	
Max. and min. transmission	0.7477 and 0.2667	0.336 and 0.081	
Data/restraints/parameters	2457/0/91	2500/0/118	
Goodness-of-fit on <i>F</i> ²	1.092	1.059	
Final <i>R</i> indices [<i>I</i> > 2 σ (<i>I</i>)]	<i>R</i> ₁ = 0.0263, <i>wR</i> ₂ = 0.0691	<i>R</i> ₁ = 0.0369, <i>wR</i> ₂ = 0.0794	
<i>R</i> indices (all data)	<i>R</i> ₁ = 0.0272, <i>wR</i> ₂ = 0.0700	<i>R</i> ₁ = 0.0480, <i>wR</i> ₂ = 0.0870	
Largest diff. peak and hole	3.104 and -2.456 e Å ⁻³	2.736 and -1.407 e Å ⁻³	
Structure	12	13	
Abbreviation	[Hg(μ -Br) ₂ (quin)] _∞	[Hg ₂ (μ -I) ₂ I ₂ (quin) ₂]	
Empirical formula	C ₉ H ₇ NHgBr ₂	C ₁₈ H ₁₄ N ₂ Hg ₂ I ₄	
Formula weight (g mol ⁻¹)	489.57	1167.09	
Temperature	293(2) K	293(2) K	
Wavelength	0.71073 Å	0.71073 Å	
Crystal system	Triclinic	Triclinic	
Space group	<i>P</i> $\bar{1}$	<i>P</i> $\bar{1}$	
Unit cell dimensions	<i>a</i> = 7.6214(10) Å <i>b</i> = 7.6716(11) Å <i>c</i> = 10.0092(14) Å	<i>a</i> = 8.0024(5) Å <i>b</i> = 8.7714(6) Å <i>c</i> = 9.5211(6) Å	

Table 2 (continued)

Structure	12	13
	$\alpha = 112.155(3)^\circ$	$\alpha = 86.141(2)^\circ$
	$\beta = 91.133(3)^\circ$	$\beta = 67.909(2)^\circ$
	$\gamma = 91.574(3)^\circ$	$\gamma = 71.203(2)^\circ$
Volume	541.52(13) Å ³	585.11(7) Å ³
Z	2	1
Density (calculated)	3.002 Mg m ⁻³	3.312 Mg m ⁻³
Absorption coefficient	21.542 mm ⁻¹	18.385 mm ⁻¹
F(000)	436	508
Crystal size	0.244 × 0.204 × 0.100 mm ³	0.311 × 0.063 × 0.033 mm ³
Theta range for data collection	2.675 to 26.370°	2.313 to 26.360°
Reflections collected	8350	13 330
Independent reflections	2224 [$R_{\text{int}} = 0.0596$]	2383 [$R_{\text{int}} = 0.0551$]
Completeness to θ	99.9%	100.0%
Max. and min. transmission	0.7473 and 0.1873	0.5820 and 0.0690
Data/restraints/parameters	2224/33/118	2383/0/118
Goodness-of-fit on F^2	1.087	1.059
Final R indices [$I > 2\sigma(I)$]	$R_1 = 0.0402$, $wR_2 = 0.0943$	$R_1 = 0.0553$, $wR_2 = 0.1415$
R indices (all data)	$R_1 = 0.0512$, $wR_2 = 0.1006$	$R_1 = 0.0629$, $wR_2 = 0.1483$
Largest diff. peak and hole	2.132 and -0.791 e Å ⁻³	5.325 and -3.503 e Å ⁻³

parameters as well as the unit cell volume increase along the series of structures 1 to 3, and this can be ascribed to the increase in the size of the halide anion while the metal- and organic-ligand components remain constant. The a unit cell parameter, however, increases in going from structure 1 to 2, but then decreases significantly in structure 3. This decrease can be explained upon considering the difference in the ω angle of the organic ligand in structure 3, compared to those in structures 1 and 2. ω measures the rotation of the mean ring plane around the M–N bond against the $M \cdots M$ vector. The much smaller value of ω in structure 3 indicates a more rotated organic ligand, which makes the effective thickness of the polymer lower, and since the polymers stack in the a -direction, the length of the a unit cell parameter is decreased.

Selected bond lengths and angles pertaining to the metal halide-bridged polymer and the orientation of the organic ligand are listed in Table 3. The axial line ($X^{\text{ii}}\text{--M--}X^{\text{iii}}$) in all compounds is close to linear, with the axial I–Cd–I line in 3 deviating the most from 180° with an $\angle(\text{I–Cd–I})$ reflex angle of 185.44(1)°.

Relative to the halide-bridged chain, the axial line progresses from concave down in 1, to approximately linear in 2, and to concave up in 3 with the increase in size and steric requirements of the bridging halide ligand, as illustrated in Fig. 3. The axial line in compound 7, which has phenazine as the coordinating ligand, is only slightly more concave down than that observed in its acridine counterpart, compound 1. Compounds 4 and 5 follow the same trend as that observed in compounds 1–3 regarding the progression through concavity although at smaller angular increments. Both the equatorial and apical M–X bond distances increase in length with the size of the bridging halide ligands in compounds 1–3 as well as 4 and 5. The equatorial M–X bond distances which comprise the trigonal base plane are, as usual for Hg²⁺ coordination compounds,¹⁶ slightly shorter in the mercuric compounds 4 and 5 than the corresponding distances observed

in the Cd²⁺ analogues, compounds 1 and 2. When the quadrilateral bridging units are considered, the intrachain $\angle(\text{XMX})$ s as well as intrachain M(1)⋯M(2) distances increase with the size of the halide ligands, while the $\angle(\text{MXM})$ s decrease. The exaggerated effect is schematically illustrated in Fig. 4.

As is usual for Hg²⁺, the M–N distances in compounds 4 and 5 are substantially shorter than the corresponding Cd–N bond distances in compounds 1–3 and 7.¹⁷ The ω angles, which indicate the rotation of the mean ring plane through the ligand around the M–N bond as measured against the $M \cdots M$ vector, are 71.3(6)°, 69.0(3)° and 62.9(2)° for 1, 2 and 3, respectively, and decrease, indicating a larger degree of organic ligand rotation, with an increase in size of the halide ligand, as illustrated in Fig. 5, and thus the repeat length of the polymer, in order to maintain a similar distance between the acridine ligands that is conducive to aromatic interactions, which will be discussed later. The same holds true for the ω angles in 4 and 5, while 7, the only phenazine-containing polymer in this series, has the largest ω angle at 73.0(2)°.

The two equal $\angle(\text{XMN})$ angles in the trigonal base plane open up with an increase in size of the halide ligand in the Cd-containing compounds 1–3, with concomitant closing of the $\angle(\text{XMX})$ angle in the plane, as illustrated in Fig. 6.

This is ascribed to a decrease in the ω angle, as discussed earlier, which rotates the mean plane through the organic ligand onto the equatorial plane of the trigonal bipyramidal metal centre, with increasing size of the halide ligand, as schematically presented in Fig. 6. As the ω angle decreases, the $\angle(\text{C}(2)\text{--H}(2)\text{--X}(1))$ angle progresses from 162.8° in 1, to 166.4° in 2, and to 173.5° in 3, and as the C–H functionality moves closer to the larger X(1) bridging ligand, concomitant steric requirements therefore necessitate closing of the $\angle(\text{XMX})$ angle. This effect is especially pronounced in going from compound 2 to 3, where a larger change in the ω angle than that noticed upon comparing compounds 1 and 2 is observed, thus requiring a larger decrease in the equatorial

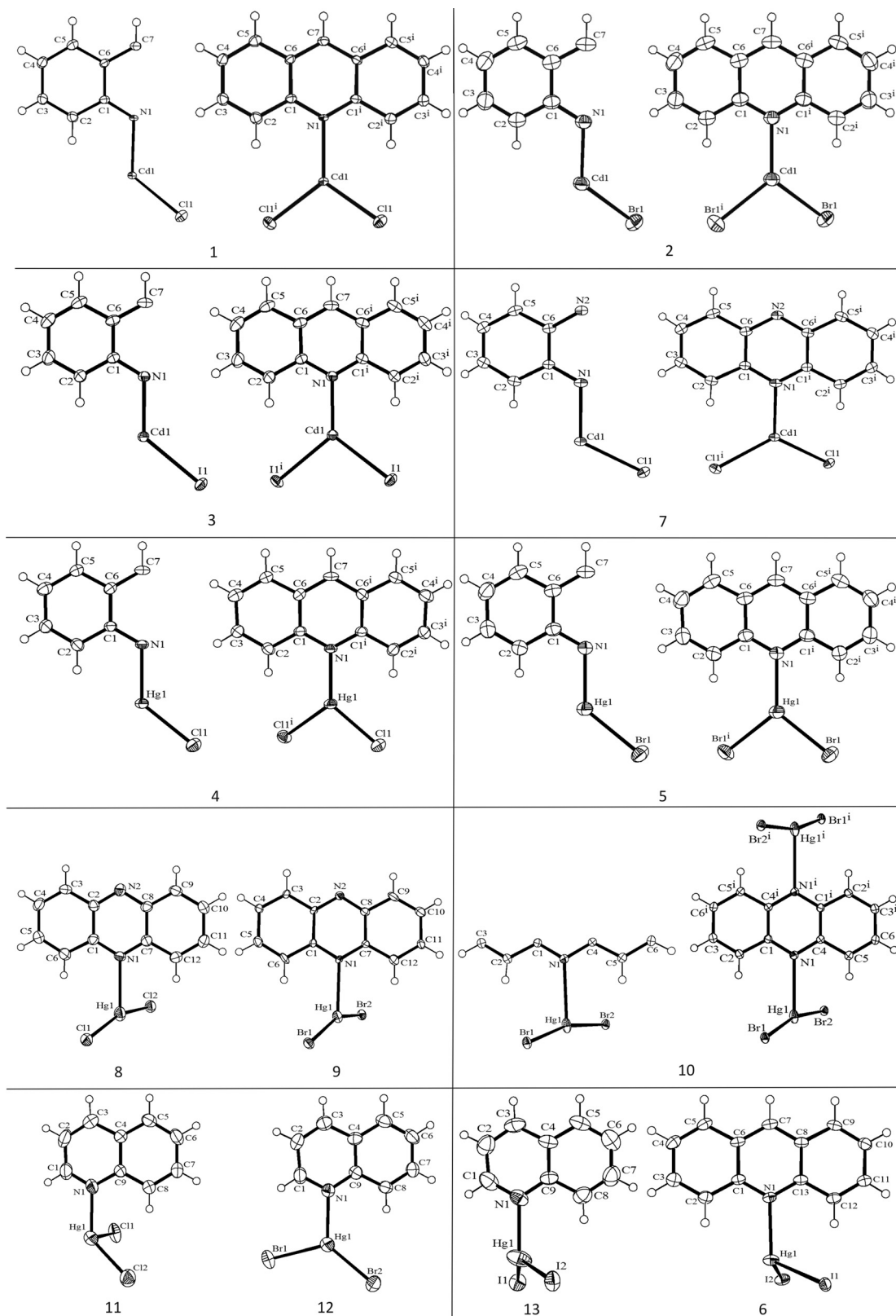


Fig. 1 Asymmetric units of 1–13 (left). Repeating motifs, generated from the asymmetric unit by a two-fold rotation axis with direction $[0, 1, 0]$, showing the atomic numbering scheme of symmetry-generated atoms to the right of each asymmetric unit. ⁱ represents the symmetry operator, $1 - x, y, 3/2 - z$, in compounds 1–5 and 7, and $1 - x, 1 - y, 2 - z$, in compound 10 used to generate equivalent atoms. Displacement ellipsoids are shown at the 50% probability level, and hydrogen atoms are shown as small spheres of arbitrary radii.

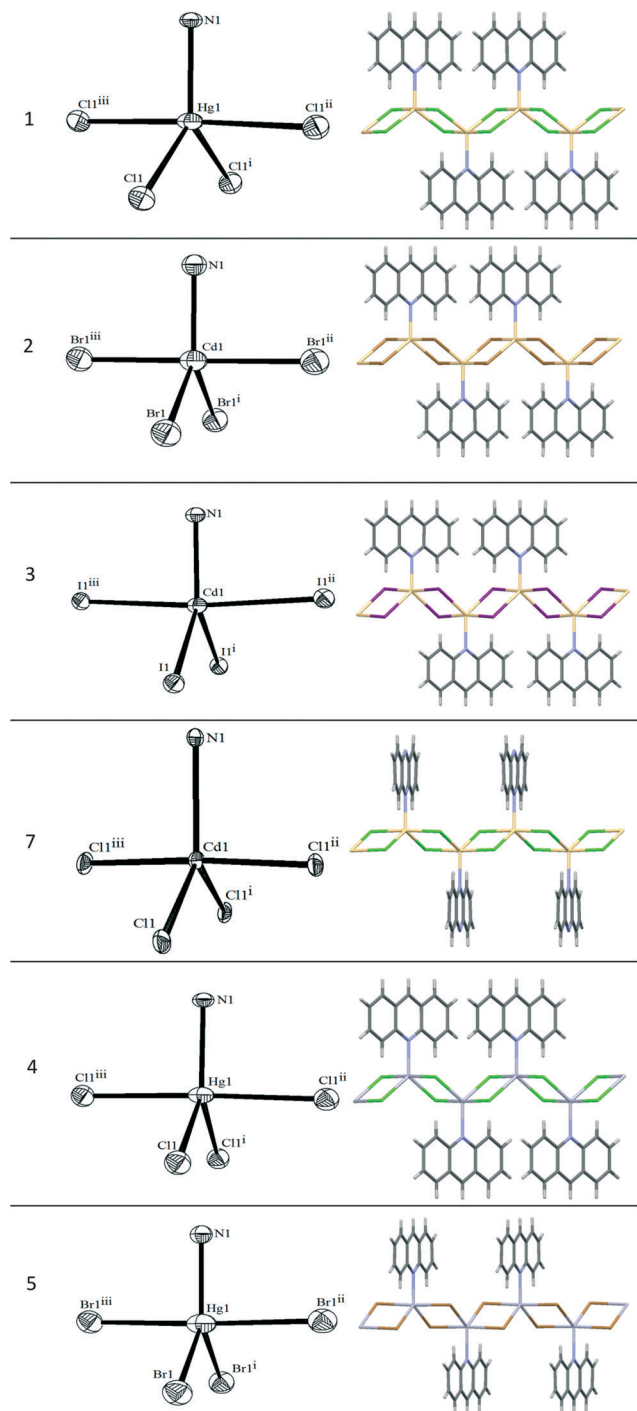


Fig. 2 Metal coordination spheres in compounds 1–5 and 7, with $M = \text{Cd}^{2+}$ in 1–3 and 7, and $M = \text{Hg}^{2+}$ in 4 and 5 (left). Section of one-dimensional halide-bridged polymers of compounds 1–5 and 7 viewed along the crystallographic a -axis (right). Symmetry operators used to generate equivalent atoms: ⁱ $1 - x, y, 3/2 - z$, ⁱⁱ $x, 1 - y, 1/2 + z$, ⁱⁱⁱ $1 - x, 1 - y, 1 - z$.

$X-M-X$ angle. This is, however, not observed in the Hg^{2+} compounds 4 and 5, where the $\angle(XMN)$ and $\angle(XMX)$ angles remain approximately equal upon increasing the size of the halide ligand, due to the more flexible coordination sphere inherent to the Hg^{2+} metal centre.

Table 3 Selected bond lengths and angles in 1–5 and 7 (\AA , $^\circ$), $M = \text{Cd}$ (1–3, 7), Hg (4, 5) and $X = \text{Cl}$ (1, 4, 7), Br (2, 5), I (3). $M(1)$ and $M(3)$ refer to co-linear metal centres related by translation, while $M(1)$ and $M(2)$ refer to neighbouring metal centres related by inversion and connected via bridging halide ligands

	1	2	3
Apical $M-X$ (\AA)	2.675(3)	2.8235(7)	3.0191(3)
Axial $X-M-X$ ($^\circ$)	177.73(7)	180.31(2)	185.44(1)
Equatorial $M-X$ (\AA)	2.504(2)	2.6343(8)	2.8238(3)
Equatorial $X-M-X$ ($^\circ$)	110.56(7)	107.24(2)	103.44(1)
Equatorial $X-M-N$ ($^\circ$)	124.7(2)	126.4(1)	128.28(5)
$M-N$ (\AA)	2.274(8)	2.288(4)	2.298(2)
$M(1)\cdots M(3)$ (\AA)	7.0529(9)	7.2771(4)	7.6053(3)
$M(1)\cdots M(2)$ (\AA)	3.8241(5)	3.9569(3)	4.1279(2)
ψ ($^\circ$)	90.00	90.00	90.00
θ ($^\circ$)	90.00	90.00	90.00
ω ($^\circ$)	71.3(6)	69.0(3)	62.9(2)
Intrachain $X-M-X$ ($^\circ$)	84.86(7)	87.13(2)	90.17(1)
Intrachain $M-X-M$ ($^\circ$)	95.14(7)	92.87(2)	89.83(1)
	7	4	5
Apical $M-X$ (\AA)	2.6267(7)	2.880(4)	3.0146(5)
Axial $X-M-X$ ($^\circ$)	176.79(3)	177.77(8)	182.19(1)
Equatorial $M-X$ (\AA)	2.5148(7)	2.476(2)	2.5900(4)
Equatorial $X-M-X$ ($^\circ$)	121.00(3)	104.39(9)	104.25(1)
Equatorial $X-M-N$ ($^\circ$)	119.50(8)	127.8(3)	127.9(1)
$M-N$ (\AA)	2.311(3)	2.21(1)	2.244(4)
$M(1)\cdots M(3)$ (\AA)	7.0588(3)	7.1913(2)	7.4205(5)
$M(1)\cdots M(2)$ (\AA)	3.7653(2)	3.9251(2)	4.0143(3)
ψ ($^\circ$)	90.00	90.00	90.00
θ ($^\circ$)	90.00	90.00	90.00
ω ($^\circ$)	73.0(2)	69.5(8)	67.3(3)
Intrachain $X-M-X$ ($^\circ$)	85.86(2)	86.06(8)	88.83(1)
Intrachain $M-X-M$ ($^\circ$)	94.14(2)	93.94(9)	91.17(1)

The equatorial plane of the trigonal bipyramidal metal centre in 7, the only phenazine analogue in the series,

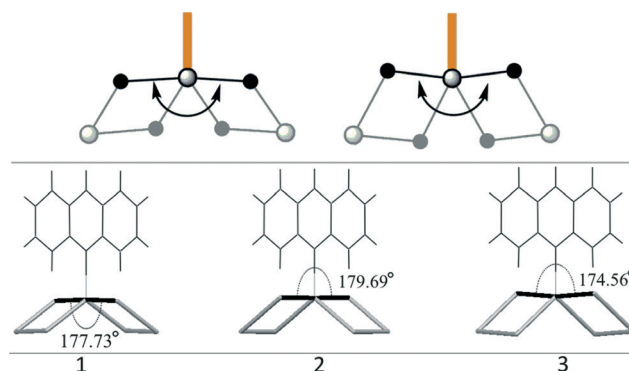


Fig. 3 Schematic representation of concave down and concave up axial $X-M-X$ angles (top). Progression of the axial $X-M-X$ line (highlighted in black) from concave down in 1 ($X = \text{Cl}$), close to linear in 2 ($X = \text{Br}$), to concave up in 3 ($X = \text{I}$) (bottom). The obtuse angle is indicated in all instances.

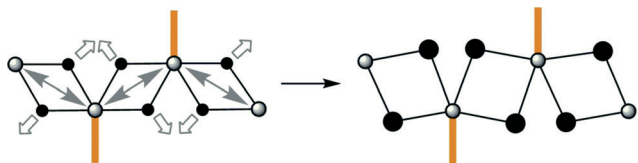


Fig. 4 Exaggerated schematic representation of the effect of increase in halide ligand (black spheres) size on intrachain bridging-unit $\angle(XMX)$ and $\angle(MXM)$ parameters.

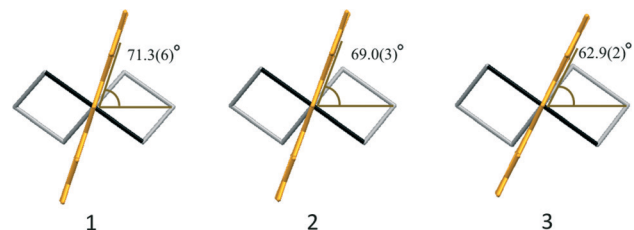


Fig. 5 Clockwise rotation of the organic ligand (orange) around the Cd-N bond showing the decrease in ω angle with the increase in size of the halide ligand in 1-3.

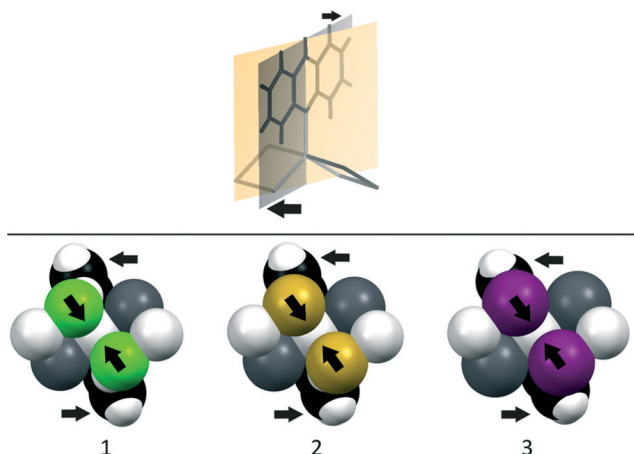


Fig. 6 Graphical representation of the mean plane through the organic ligand (grey) approaching the equatorial plane (orange) of the trigonal pyramid as the ω angle decreases with an increase in size of the halide ligand (top). Decrease in both $\angle(XMX)$ and ω angles with increasing halide ligand size (bottom). Chloride ligands are represented in lime, bromide ligands in gold and iodine ligands in purple.

approaches a near perfect trigonal planar geometry with the $\angle(\text{Cl}-\text{Cd}-\text{Cl})$ angle and the two $\angle(\text{Cl}-\text{Cd}-\text{N})$ bond angles at $121.00(3)^\circ$ and $119.50(8)^\circ$, respectively. The corresponding angles in polymers 1-5, however, deviate significantly from 120° .

At $2.311(3) \text{ \AA}$, the M-N bond distance in 7 is slightly larger than that observed in the acridine analogues 1-5. This may be the result of a long range $\text{M}\cdots\text{N}$ interaction, at 4.862 \AA , with a Cd^{2+} metal centre in a neighbouring polymer along the *b*-direction, *via* the uncoordinated N(2) atom of the phenazine ligand, as illustrated in Fig. 7, which is not possible in compounds 1-5 due to the ligand being acridine. Both ψ and θ in all compounds approximate 90° , which means that the

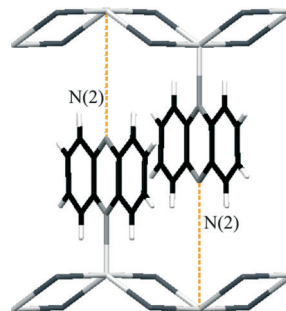


Fig. 7 Additional long-range $\text{M}\cdots\text{N}$ interactions (orange) between Cd^{2+} metal centres in neighbouring polymer chains along the *b*-direction *via* the uncoordinated N(2) atoms of the phenazine ligands in structure 7.

M-N line as well as the mean ring plane through the organic ligand is perpendicular relative to the $\text{M}\cdots\text{M}$ vector. The effect of increasing steric demand of the halide ligand, with a concomitant decrease in the respective ω angles, is also reflected in the weak intrachain C-H \cdots μ -X-M hydrogen bonding parameters, as collated for the C(2)-H(2) \cdots X(1) interactions in Table 8.

Hydrogen bonds were defined using the default definition in Mercury,¹⁸ set to include the presence of a hydrogen atom on any donor atom, with the D-H \cdots A angle $\geq 120^\circ$ and the $d(\text{D}\cdots\text{A}) \leq 3.0 \text{ \AA}$. Hydrogen bonding interactions that slightly exceed the 3.0 \AA cut-off distance are considered as hydrogen contacts, provided that an interaction can be inferred upon consideration of the directionality of the said interaction.

The $d(\text{D}\cdots\text{A})$ distances in these interactions increase from 1 to 3 and from 4 to 5, with a concomitant increase in $\angle(\text{DHA})$. Positive rotation around the Cd-N bond, with an increase in size of the halide ligand, therefore not only maintains the aromatic interactions between the organic ligands, but also preserves the stabilising weak intrachain C-H \cdots μ -X-M hydrogen bonding interactions between the C(2)-H(2) functionality in the organic acridine moiety and the bridging X(1) halide ligand, as shown in Fig. 8(a) for 1. With an increase in halide ligand size, stabilising weak interchain C-H \cdots μ -X-M hydrogen bonding between the C(5)-H(5) functionality of the acridine ligand and the X(1) bridging halide ligand of a neighbouring polymer, as illustrated in Fig. 8(b), is also conserved by a change in the ω angle as the size of the halide ligand increases, the same mechanism observed in the conservation of the stabilising intrachain C-H \cdots μ -X-M hydrogen bonding. When the interchain C-H \cdots μ -X-M hydrogen bonding interactions between the H(5) atoms on the C(5) atoms in the ring systems and the X(1) bridging halide ligands contained in adjacent chains in the *b*-direction are considered, as illustrated in Fig. 8 for compound 1, both the $d(\text{D}\cdots\text{A})$ distance and the $\angle(\text{DHA})$ angle increase with an increase in size of the halide ligand. Neighbouring chains along the *b*-direction are thus connected *via* weak interchain C-H \cdots μ -X-M hydrogen bonds to ultimately form a supramolecular, two-dimensional hydrogen-bonded sheet that propagates parallel to the *bc*-plane.

The packing of compounds 1–5 and 7 is layered, forming alternating organic and inorganic monolayers parallel to the *ac*-plane, as shown for compound 4 in Fig. 9, in which the aromatic layers are highlighted in orange. Aromatic interactions zipper neighbouring polymers together, which result in the interdigitation of organic ligands in the organic layer, as can be seen when viewing the structures along the direction of chain propagation, the *c*-axis, as shown for compound 4 in Fig. 9(b). The ring interaction parameters of 1–5 and 7, as defined in PLATON¹⁹ with $d(\text{Cg}-\text{Cg}) < 6.0 \text{ \AA}$ and $\beta < 60.0^\circ$, are listed in Table 9. All the aromatic ring planes are parallel, as evidenced by the α angle of zero, but slipped relative to each other. The centroid-to-centroid distances and perpendicular distances between parallel organic moieties increase with the size of the halide ligand, due to the increase in the halide-bridged polymer repeat unit length. The slippage distance also increases with an increase in halide ligand size, indicating a smaller degree of interdigitation and further separation between neighbouring polymers along the series. As a result of the alternation of the organic ligand on different sides of the polymer as well as the interdigitation of organic ligands from neighbouring polymers, the nitrogen atoms in the aromatic rings do not overlap, but alternate in a head-to-tail packing, which is a preferred type of stacking for complexes with nitrogen-containing ligands since it minimises repulsion, as reported by Janiak.²⁰

The following sections report structures containing Hg^{2+} metal ions exclusively, and structures 4 and 5 reported in the previous section will be compared with the rest of the Hg^{2+} -containing structures as part of the overall comparison at the end.

$[\text{Hg}(\mu\text{-X})_2(\text{phe})]_\infty$ (8–9) and $[\text{Hg}_2(\mu\text{-phe})(\mu\text{-Br})_4]_\infty$ (10)

Compounds 8–10 were found to all display one-dimensional polymers consisting of distorted, edge-sharing square pyramids, and will be discussed next. The organic ligand-to-metal halide synthetic ratio of 1:1 is also displayed in structures 8 and 9; however, structure 10 was synthesised with a 1:2 ligand-to-metal halide ratio, resulting in the structure containing twice the amount of the metal halide, in comparison to structures 1–5 and 7–9, indicating that in some instances, the structure can be controlled by the stoichiometric ratio of the reagents.

The asymmetric units of the isostructural compounds, 8 and 9, consist of a distorted square pyramidal Hg^{2+} ion coordinated to two halide ligands, chloride in 8 and bromide in 9, and one phenazine ligand coordinated *via* one nitrogen atom only, as illustrated in Fig. 1. The asymmetric unit of 10, as shown in Fig. 1, contains one distorted square pyramidal Hg^{2+} ion coordinated to two bromide ligands and half a phenazine ligand, and the full repeat unit is generated by operation of an inversion centre positioned at (0, 0, 0). Compounds 8–10 all crystallise in the triclinic space group $P\bar{1}$ and their crystallographic parameters are listed in Table 2. None of the atoms in compounds 8–10 occupy special positions, with two asymmetric units comprising each unit cell.

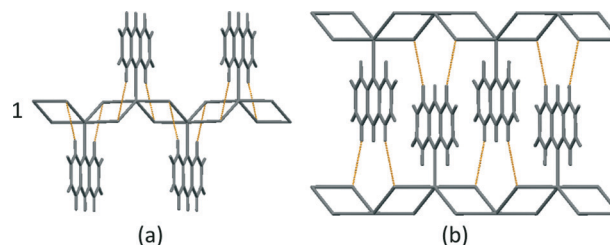


Fig. 8 (a) Weak intrachain C–H⋯μ–X–M hydrogen bonding interactions between the acridine ligands and the bridging halide ligands comprising the trigonal base plane in 1, as viewed perpendicular to the direction of chain propagation. (b) Weak interchain C–H⋯μ–X–M hydrogen bonding interactions between neighbouring chains in 1, as viewed perpendicular to the direction of chain propagation.

In compounds 8–10, the adjacent metal centres, coordinated by an inversion centre at [0, 0, 0], are bibriged by two halide ligands which connect the five-coordinate Hg^{2+} ions as distorted edge-sharing square pyramids to form one-dimensional halide-bridged chains. The metal centres are above the square base plane formed by the four halide ligands, as illustrated in Fig. 10(a). The chains extend along the direction of the shortest lattice parameter, the *a*-axis, with the distance between co-linear mercury ions equal to the *a* cell spacing. The *a* unit cell parameter in 10 is approximately half of those observed in 8 and 9. The smaller value reflects the scalloped chain conformation (Scheme 2, right) adopted by 10, in which co-linear metal centres are also adjacent ($\text{M}(1)\cdots\text{M}(2)$), as opposed to the zigzag ribbon motif (Scheme 2, left) adopted by 8 and 9, in which co-linearity is observed between every second metal centre, $\text{M}(1)\cdots\text{M}(3)$. In compounds 8 and 9, the geometrical demand of the metal coordination sphere is satisfied by coordination of one nitrogen atom of the phenazine ligand in the apical position. The phenazine ligands alternate between the ‘above’ and ‘below’ positions along the halide-bridged chain when viewed perpendicular to the direction of chain propagation, as illustrated in Fig. 10(b). However, in compound 10, the phenazine ligand coordinates *via* both nitrogen atoms, as illustrated in Fig. 10, to extend the one-dimensional halide-bridged chain

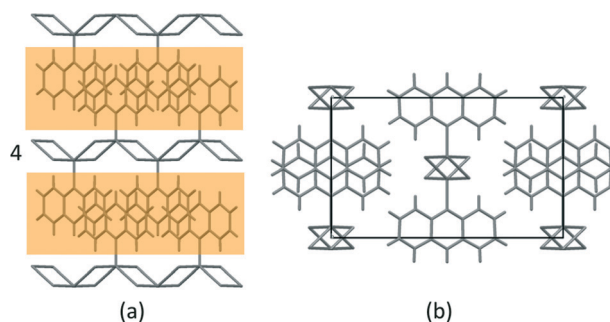


Fig. 9 (a) Layered packing arrangement of 4 as viewed down the crystallographic *a*-axis. The organic layers are highlighted in orange. (b) Packing arrangement of 4 as viewed down the crystallographic *c*-axis.

in the *c*-direction to form a double-chain phenazine sandwich. The phenazine ligand therefore acts as a ditopic ligand by having both nitrogen atoms ligated to symmetry-related metal centres, and the organic ligand no longer alternates above and below the halide-bridged chain, but all occur on the same side of the chain. In compound **10**, the overall chain conformation can be likened to a one-dimensional ladder, with the phenazine ligands forming the rungs and the halide-bridged chains constituting the rails. The position of the metal centre relative to the inversion centre in **8–10** results in four unequal Hg–X (X = Cl in **8**, Br in **9** and **10**) bond lengths around each metal centre. In compounds **8** and **9**, each bridging quadrilateral forms a parallelogram, comprising two longer and two shorter Hg–X bond distances, as collated in Table 4; however, two parallelograms of different dimensions alternate positions along the chain. In compounds **8** and **9**, this results in the chain propagating in a staggered fashion, reminiscent of a houndstooth pattern. In compound **10**, the bridging quadrilateral is puckered and consists of, albeit two longer and two shorter Hg–X bond distances, four unequal side lengths.

As proposed by Englert,¹³ the halide-bridged Hg²⁺ chain can also be thought of as a repeating array of preformed HgX₂ units, linked by elongated Hg⋯X interactions, as schematically depicted in Fig. 11.

The ψ angle of **8** and **9** is similar with a very slight decrease in the parameter with an increase in size of the halide ligand in order to maintain aromatic interactions between the constituents of the organic layer by maintaining a favourable distance between them. Since the base plane of the square pyramid is not co-planar with the metal centre, but below or above it at distances of 0.456 Å and 0.613 Å for **8** and **9**, respectively, ψ is measured as $\angle(\text{N1-Hg1-Hg3})$, as schematically presented in Scheme 1, a1. The base plane of the square pyramid in **10** is also below the metal centre, with the distance between the square base plane and the metal centre being 0.328 Å. Here, ψ is measured as $\angle(\text{N1-Hg1-Hg2})$, as schematically presented in Scheme 1, a2. Selected bond lengths and angles are given in Table 4. The Hg–N bond length in **8** and **9** decreases slightly with an increase in halide ligand size. This is opposite to the trend observed in the acridine analogues, **4** and **5**, where the Hg–N bond length increases with an increase in size of the halide ligand. The reverse observation can be explained when the geometry around the metal centres, the topicity and chemical composition of the organic donor ligands together with the size of the halide ligand are considered. In compounds **4** and **5**, the geometry around the metal centre is trigonal bipyramidal. The factors that contribute to the adopted geometry of the Hg²⁺ cations in **4** and **5** as well as **8** and **9** are both the topicity of the organic donor ligand and the nature of the donating atom. Phenazine is a ditopic N-donor organic ligand, while acridine is a monotopic N-donor ligand. In **8** and **9**, the organic ligands of neighbouring polymers interdigitate to allow for aromatic interactions between the organic ligands. However, in these structures, the Hg²⁺ metal centre's natural

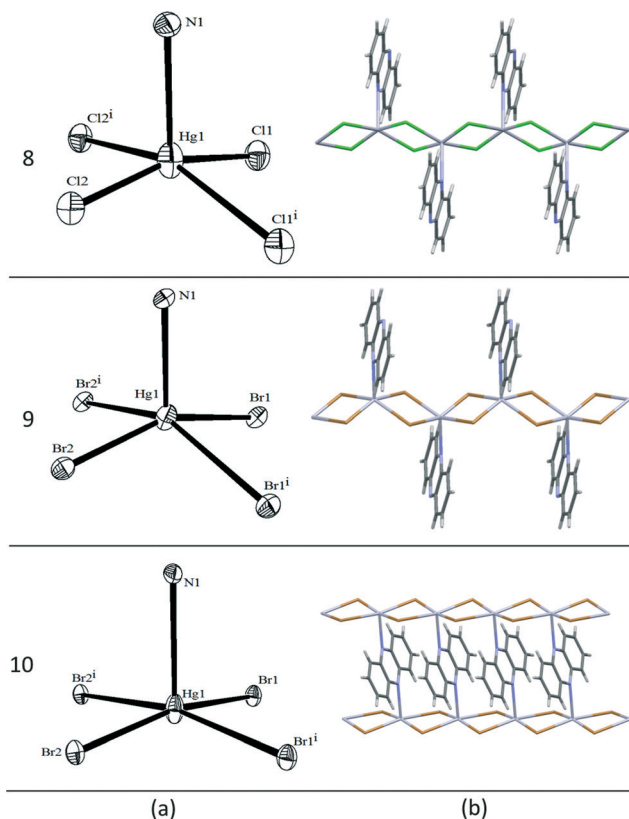


Fig. 10 (a) Five-coordinate Hg²⁺ metal centres of **8–10**, showing the numbering scheme of symmetry-generated halide ligands. (b) Section of the formed one-dimensional halide-bridged polymer in **8–10**, viewed perpendicular to the direction of chain propagation. Symmetry transformation used to generate equivalent atoms: ⁱ $-x, -y, -z$.

Table 4 Selected bond distances and angles in **8–10** (Å, °), X = Cl (**8**), Br (**9**, **10**). M(1), M(2) and M(3) refer to successive metal centres connected via bridging halide ligands

	8	9	10
Apical Hg(1)–N(1) (Å)	2.595(7)	2.563(9)	2.784(3)
Sq. base plane⋯Hg (Å)	0.456	0.612	0.328
Hg(1)⋯Hg(3) (Å)	7.7038(2)	7.9165(5)	—
Hg(1)⋯Hg(2) (Å)	3.9544(3)	4.1335(6)	4.0824(2)
ψ (°)	85.9(1)	85.3(2)	86.56(7)
θ (°)	72.2(2)	71.7(2)	67.4(1)
ω (°)	72.8(2)	71.2(3)	73.6(1)
Hg–X1 (Å)	2.334(1)	2.461(1)	2.4458(4)
Hg–X2 (Å)	2.338(2)	2.4634(9)	2.4363(4)
Hg–X2 ⁱ (Å)	3.059(2)	3.262(1)	3.1108(5)
Hg–X1 ⁱ (Å)	3.104(2)	3.296(1)	3.3527(5)
Intrachain X1–M–X2 (°)	160.19(6)	154.88(4)	164.56(2)
Intrachain X1 ⁱ –M–X2 ⁱ (°)	160.94(5)	155.75(3)	169.17(1)
Apical Hg(1)⋯N(2) (Å)	3.670(8)	4.002(9)	—

affinity for N-donor ligands¹⁷ results in the transformation of the trigonal bipyramidal geometry of the metal centre, as observed in **4** and **5**, into the pseudo-square pyramidal

geometry observed for the metal centres in **8** and **9** in order to accommodate additional long-range Hg–N interactions upon availability of an uncoordinated N-donor ligand in a neighbouring polymer, as schematically illustrated in Fig. 12, effectively changing the metal coordination geometry in **8** and **9** to pseudo-octahedral due to the presence of the long-range Hg–N interactions. This effect is not observed in structure **7**, which also contains a phenazine ligand; however, the Cd²⁺ ion in **7** does not show such an affinity for N-donor ligands. A long-range N⋯Cd²⁺ interaction is observed in **7**, but this interaction is not significant enough to change the coordination geometry from trigonal bipyramidal to square pyramidal as observed in **8** and **9**. As was mentioned, the base plane of the square pyramid is not co-planar with the metal centre, but below or above it at distances of 0.456 Å and 0.6127 Å for **8** and **9**, respectively. This increase in distance can be understood by acknowledging the increasing size of the halide ligand with a simultaneous decrease in the ω angle. Concomitant intrachain $\angle(X1-M-X2)$ and $\angle(X1^i-M-X2^i)$ angles of *ca.* 160.57° for **8** and *ca.* 155.32° for **9** result in the Hg²⁺ metal cation in **8** being sterically less hindered than the Hg²⁺ metal cation in **9**, and **8** can therefore better accommodate the second, semi-coordinated nitrogen atom of the phenazine ligand of a neighbouring polymer along the *b*-direction coming into contact. The resulting long-range interchain Hg(1)⋯N(2) interactions between the second nitrogen atom of the phenazine ligand and the Hg²⁺ metal cation in a neighbouring polymer bring about the slightly elongated Hg(1)–N(1) bond observed in **8** in comparison to the corresponding distance in **9**. The interdigitated phenazine ligands may be seen to form short contacts with the Hg²⁺ metal centres of the adjacent chains *via* the N(2) atom, with Hg⋯N(2) distances of 3.669(8) Å and 4.002(9) Å for **8** and **9**, respectively. Compound **10** has, at 2.784(3) Å, the longest Hg–N bond which can be understood by following the reasoning given above.

The packing arrangement in compounds **8** and **9** is layered with alternating organic and inorganic monolayers parallel to the *bc*-plane. As was the case for compounds **1–5** and **7**, molecular zipping between neighbouring chains in the *b*-direction in compounds **8** and **9** results from both aromatic interactions between the organic ligands in the neighbouring chains in the organic layer and weak interchain C–H⋯ μ -X–M hydrogen bonds. The organic layers in the said packing arrangements are thus highly interdigitated, as illustrated in the interchain packing diagram of **9** shown in Fig. 13(a), in which alternating layers are given in grey and black to highlight the extent of interdigitation between the phenazine ligands in neighbouring one-dimensional chains. As

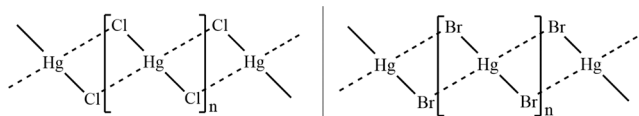


Fig. 11 Schematic representation of asymmetric Hg–X bonding, suggestive of preformed HgX₂ units in compounds **8** (left) and **9** (right).

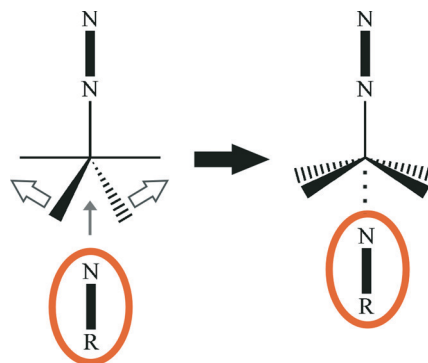


Fig. 12 Schematic illustration of a trigonal bipyramidal Hg²⁺ metal centre approaching square planar geometry upon availability of an N-donor ligand.

anticipated from the different dimensions of successive bridging parallelograms that alternate positions along the chain, the symmetry results in two alternating centroid-to-centroid distances in both **8** and **9**.

Centroid-to-centroid, perpendicular and slippage distances between parallel phenazine moieties in compounds **8** and **9** increase with the size of the halide ligand, as a result of the increase in the number of polymer repeat units and the lower degree of interdigitation. The ring interaction parameters of **8–10** are listed in Table 9. The packing arrangement adopted by **10** is shown in Fig. 13(c) and (d) as viewed down the *b*- and *a*-axes, respectively. The packing is layered, forming alternating organic and inorganic layers parallel to the *bc*-plane. The centroid-to-centroid distance between the phenazine rings in the organic layer is constant at 4.082(2) Å, which is comparable to the corresponding distances observed in **9**. The perpendicular slippage distance between parallel organic moieties is, however, 2.008 Å in **10**. This distance is noticeably larger in comparison to the distance of 1.864 Å observed in compound **9**. This is due to the fact that in compounds **8** and **10**, the aromatic interactions occur between interdigitated phenazine ligands from adjacent chains (inter-aromatic interactions), which is not the case in **10**, where aromatic interactions occur between ditopic phenazine ligands from the same chain (intra-aromatic interactions). Since the intrachain distance between the host metal centres is, at 4.0824(2) Å, the limiting factor, the maintenance of a favourable distance for aromatic interactions is achieved by an increase in the ψ and ω angles of 86.56(7)° and 73.6(1)°, respectively, a decrease in the θ angle of 67.4(1)°, as listed in Table 4, and the kink observed in the bridging unit. Compared to structures **8** and **9**, the packing arrangement is such that the inorganic layer can be seen to form a double chain, as illustrated in Fig. 13(c) and (d). In this double metal-halide chain, the bromide ligands are positioned above the Hg²⁺ ions, resulting in electrostatically stabilised, semi-coordinate Hg⋯Br close contacts.

The values of the θ angles in compounds **8–10** range between 67.4(1)° and 72.2(2)°, while the ψ angles range between 85.3(2)° and 86.56(7)°. These values are considerably

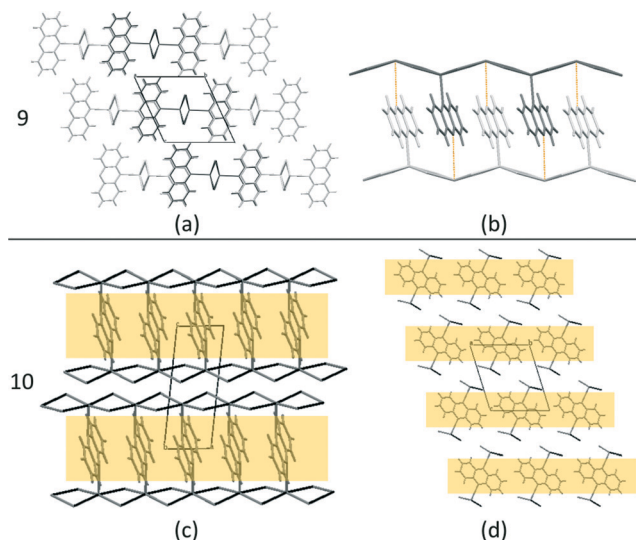


Fig. 13 (a) Projection of **9** along the [100] direction, with alternating layers shown in grey and black, which is also representative of structure **8**. (b) Short Hg \cdots N(2) contacts (in orange) between adjacent chains of **9** as viewed perpendicular to the direction of chain propagation. These interactions are also observed in **8**. (c) Packing arrangement of **10** as viewed down the crystallographic *b*-axis. (d) Packing arrangement of **10** as viewed down the crystallographic *a*-axis. The organic layers are highlighted in orange.

lower in comparison to the corresponding θ and ψ angles observed in compounds **1–5** and **7**. This effect can be rationalised when the topicity of the organic ligand, the nature of the metal centre and the aromatic interactions between aromatic moieties in the respective organic layers are again considered. The decreased ψ angles in **8–10**, in comparison to those observed in compounds **1–5** and **7**, seem to be resulting from the decreased θ angles as a side effect. The θ angles decrease in order to maintain a parallel displaced orientation conducive to aromatic interactions between the interdigitated phenazine ligands. Due to the short interchain Hg \cdots N(2) contacts in compounds **8** and **9**, and the ditopic binding mode of the phenazine ligand in **10**, the phenazine ligands are anchored more strongly in a specific position between metal halide chains, and cannot slip relative to each other in either the *b*- (as was the case in compound **7**) or *c*-directions, in order to maintain an offset-stacked arrangement. The only way in which such an arrangement can be maintained is therefore by decreasing the θ angle. In compound **7**, the metal centre comprise a Cd²⁺ cation, whose natural affinity for N-donor organic ligands is much lower than that of a Hg²⁺ cation,¹⁷ which means that no second, semi-coordinate Cd \cdots N contact with the organic ligand is present, and that the organic ligands can adopt a more slipped arrangement. Weak intrachain C–H \cdots μ -X–M hydrogen bonds are present in compounds **8** and **9** between the C(12)–H(12) and C(6)–H(6) functionalities of the phenazine ligands and the X(1) and X(2) halide ligands in the same polymer, respectively. The corresponding interactions in compound **10** are between the C(2)–H(2) and C(5)–H(5) functionalities and the Br(2) and Br(1) ligands. These

interactions further link the repeating HgX₂ (X = Cl, Br) units described previously by forming C–H \cdots μ -X–Hg bonds to the bridging halide ligands furthest from the metal centre, and therefore contribute to the inter-unit linkage, as illustrated in Fig. 14. These interactions are not symmetric around the respective metal centres due to the asymmetric nature of the bridging halide units comprising the halide-bridged chains. The asymmetric bridging units also seem to be responsible for the side-way tilt observed in the phenazine ligand relative to the halide-bridged chain in compounds **8–10**. The formation of these contacts, together with the maintenance of a favourable distance between organic moieties for aromatic interactions with an increase in size of the halide ligand, necessitates the observed ω angles of 72.8(2) $^\circ$ and 71.2(3) $^\circ$ for **8** and **9**, respectively.

Weak interchain C–H \cdots μ -X–M hydrogen bonding interactions between the H(3) and H(12) atoms on the C(3) and C(12) atoms of the organic ligand, respectively, in both **8** and **9**, and the bridging halide atoms in a neighbouring chain form a two-dimensional hydrogen-bonded network along the *ab*-plane, as shown in Fig. 14(b). The weak interchain C–H \cdots μ -X–M hydrogen bonds together with the interchain Hg(1) \cdots N(2) short contacts also contribute to the observed θ angles to ensure optimal space filling to maintain the inter-aromatic interaction bond distances. Hydrogen bonding parameters are listed in Table 8. The corresponding hydrogen bonds in **10** fulfill the same function as those observed in **8** and **9**, as illustrated in Fig. 14(d), with imposed ω and θ angles listed in Table 4; however, in this case, the interactions are intrachain. Extension of interchain Hg(1) \cdots Br(1) contacts along the *bc*-plane in compound **10** (see Fig. 15(a)) links the neighbouring inorganic monolayers into the stacked-ribbon conformation schematically depicted in Fig. 15(b). The Hg(1) \cdots Br(3) contact distances are 3.5730(4) Å.

Weak interchain C–H \cdots μ -X–M hydrogen-bonded short contacts of 3.0508 Å between the H(3) ring hydrogens and the bridging Br(2) ligands in adjacent chains further promote association between neighbouring chains in the *b*-direction and also directs the positioning of the neighbouring chains to aid in interchain close packing of the spherical bromide ligands, as illustrated in Fig. 15(d).

The question that remains is why does the distorted square pyramidal base in **10** not flatten out completely to form a moiety in which the base plane is coplanar with the metal centres, upon forming the stacked-ribbon supramolecular motif, to form the formal stacked-ribbon motif, as schematically shown in Fig. 15(b), instead?

Three related structures in which Hg²⁺ presents the stacked-ribbon supramolecular motif are available in the literature: QEZNOA,²¹ QUMVEA¹⁰ and SAXDOK,²² with *N*-(3-chlorophenyl)pyrazine-2-carboxamide, 3,5-dimethylpyrazine and 2-methylquinoxaline as the respective N-donor ligands. These structures are not of the sandwich-type, and the ligands are not coordinated ditopically. To our knowledge, compound **10**, together with QUMTUA¹⁰ and QUIMVIE,¹⁰ is the only compound of this type, exhibiting the phenazine-

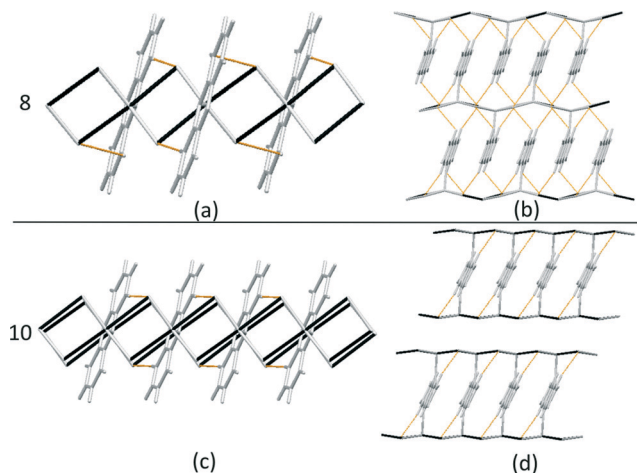


Fig. 14 (a) Intrachain hydrogen bonding interactions between HgCl_2 units in **8** viewed along the b -axis. (b) Two-dimensional hydrogen-bonded network in **8** as viewed along the c -axis. (c) and (d) Intrachain hydrogen bonding interactions between HgBr_2 units in **10** as viewed from different angles perpendicular to the direction of chain propagation. The two longer $\text{M}\cdots\text{X}$ interactions comprising the quadrilateral bridging units are indicated in black.

sandwiched, stacked-ribbon supramolecular motif, deposited in the CSD.¹⁵ The distance between the square base plane and the Hg^{2+} ion does decrease substantially from 0.612 Å in **9** to 0.328 Å in **10**, indicating progression in that direction. A feasible explanation seems to be the maintenance of the aromatic interactions between rung-phenazines in conjunction with the size of the metal ion. Manipulation of the ω , ψ and θ angles to maintain a distance conducive to aromatic interactions between phenazine moieties has already been explained. Should the bridging bromide ligands now move into the plane of the metal centres to form a flat stacked-ribbon motif, the distance between the co-planar Hg^{2+} ions will have to increase, with a concomitant loss of the said aromatic interactions.

$[\text{Hg}(\mu\text{-X})_2(\text{quin})]_\infty$ (**11**–**12**)

Two compounds containing the asymmetric organic ligand quinoline, which both display edge-sharing trigonal bipyramids, were determined in this investigation. Compounds **11** and **12** are isostructural and crystallise in the triclinic space group $P\bar{1}$, and all crystallographic parameters are listed in Table 2. These structures exhibit an organic ligand-to-metal halide ratio of 1 : 1, which reflects the ratio used synthetically. The asymmetric units of **11** and **12** each consist of a trigonal bipyramidal Hg^{2+} ion coordinated to two halide ligands and one quinoline ligand *via* the nitrogen atom, as illustrated in Fig. 1. Two asymmetric units comprise each unit cell with none of the atoms in special positions.

Translation of the asymmetric unit along the a -direction connects the five-coordinate Hg^{2+} metal centres as edge-sharing trigonal bipyramids to form one-dimensional halide-bridged chain polymers, as illustrated in Fig. 16 (right). Two halide ligands together with the nitrogen atom of the organic

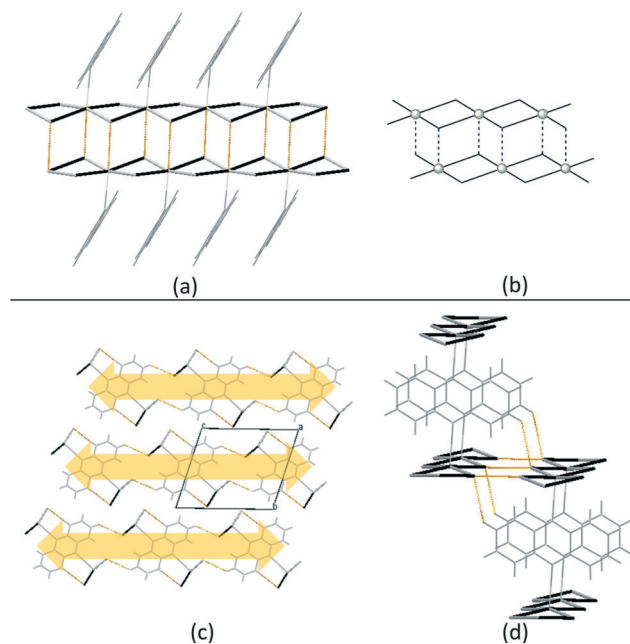


Fig. 15 (a) Interchain $\text{Hg}\cdots\text{Br}$ contacts in **10**, reminiscent of a stacked-ribbon structural motif. (b) Schematic representation of the stacked-ribbon structural motif constructed from HgBr_2 units. Weak interchain hydrogen bonding as viewed down the crystallographic a -axis (c) and slightly tilted along the same axis (d).

quinoline ligand form the trigonal base plane, with the two halide ligands coordinated in the apical positions to satisfy the geometric requirements of the five-coordinate metal centre. The chain propagates along the direction of the shortest lattice parameter, the a -axis. The distance between the co-linear mercury atoms is also equal to the a cell spacing in **11** and **12**. The b and c unit cell parameters, together with the unit cell volume, increase with the size of the halide ligand in compounds **11** and **12**. As was the case in the analogous acridine compounds, **4** and **5**, the chain adopts the zigzag ribbon motif as illustrated in Scheme 2. The planar asymmetric quinoline ligands alternate between the 'above' and 'below' positions on successive metal centres as well as between sides to which the benzo-part of the asymmetric ligand above and below protrudes relative to the halide-bridged chain when viewed perpendicular to the direction of chain propagation, as illustrated in Fig. 16 (right). The benzo-rings face furthest away from the polymer chain, and the quinoline ligands on the same side of the polymer show the same orientation. Selected bond lengths and angles are given in Table 5. As was observed in compounds **1**–**5** and **7**, the axial $\text{X}(1)\text{--Hg--X}(2)$ line of the trigonal bipyramidal metal centre deviates from 180° . However, the resulting curve cannot be described as either concave up or concave down relative to the halide-bridged chain as was the case in compounds **1**–**5** and **7**. In compounds **11** and **12**, the curve has to be described relative to the position of the benzo-part of the quinoline ligand. Due to the asymmetry of the organic ligand, the halide-bridged chain consists of a sterically hindered side (the benzo-side) and a sterically uncluttered or

open side. The axial X(1)–Hg–X(2) line, in both **11** and **12**, curves towards the uncluttered side, as illustrated in Fig. 17 and as evident from the small $\angle(X-M-N)$ angles of $105.8(4)^\circ$ and $105.9(2)^\circ$ in the base plane of the trigonal bipyramidal metal centres of both compounds **11** and **12**, respectively. The asymmetric nature of the quinoline ligand also affects the Hg(1)–N(1)–C(3) line. At values of $177.3(9)^\circ$ and $175.8(4)^\circ$ for **11** and **12**, respectively, the curve in the Hg(1)–N(1)–C(3) line serves a steric function in that it tilts in such a way as to project the benzo-part of the ligand away from the halide-bridged chain. This angular value decreases with an increase in size of the halide ligand. As was the case in compounds **8** and **9**, none of the halide ligands, either equatorially or apically positioned around the Hg²⁺ metal centre, are equidistantly coordinated. The bridging units that comprise the polymeric backbone are therefore asymmetric with a substantial difference in pairwise Hg–X (X = Cl, Br) inter-unit side lengths, resulting in two parallelograms of different dimensions alternating along the direction of chain propagation.

The two longer bond lengths belong to the apical Hg–X bonds, while the two shorter lengths correspond to the Hg–X bonds comprising two legs of the base plane of the trigonal bipyramidal Hg²⁺ metal centre. As was seen in compounds **1**–**3**, both the intrachain $\angle(XMX)$ s and the intrachain M(1)⋯M(2) distances within the bridging units increase with the size of the halide ligands, while the $\angle(MXM)$ s decrease. Since the chain consists of two different bridging units, the chain propagates in a staggered, houndstooth fashion.

The size difference between successive ribbon loops is illustrated in Fig. 18. The pairwise discord in bond lengths is indicative of preformed HgX₂ units, which are linked by the longer apical Hg(1)⋯X interactions, as proposed by Englert¹³ and seen in the other *P* $\bar{1}$ polymers **8**–**10**.

Weak intrachain C–H⋯ μ -X–M hydrogen bonds are present between the H(8) atoms of the C(8) atoms in the benzo-part

Table 5 Selected bond distances and angles in **11** and **12** (Å, °), M = Hg, X = Cl (**11**), Br (**12**)

	11	12
Apical M–X (Å)	2.858(6), 3.032(6)	2.973(1), 3.193(1)
Apical X–M–X (°)	172.6(2)	172.22(3)
Equatorial M–X (Å)	2.387(7), 2.460(7)	2.499(1), 2.5819(9)
Equatorial X–M–X (°)	125.7(2)	126.22(4)
Equatorial X–M–N (°)	105.8(4), 127.9(4)	105.9(2), 127.2(2)
M–N (Å)	2.24(1)	2.263(9)
M(1)⋯M(3) (Å)	7.394(2)	7.621(1)
M(1)⋯M(2) (Å)	3.896(1)	4.0160(7)
ψ (°)	86.7(4)	86.4(2)
θ (°)	84.7(6)	85.2(3)
ω (°)	71.0(2)	71.5(7)
Intrachain X–M–X (°)	88.9(2), 86.7(2)	89.44(3), 91.14(3)
Intrachain M–X–M (°)	93.3(2), 91.1(2)	88.86(3), 90.56(3)

of the quinoline ligands and the bridging X(2) halide ligand of the trigonal base plane and contribute to the observed ω angles of $74.0(1)^\circ$ and $71.5(7)^\circ$ for **11** and **12**, respectively.

As was the case in compounds **1**–**5** and **7**–**10**, the ω angle decreases with an increase in size of the bridging halide ligand, and positive rotation around the Hg–N bond therefore allows for the maintenance of both the C(8)–H(8)⋯ μ -X(2) hydrogen bonds and the distance between interdigitated organic moieties for retention of stabilising aromatic interactions. The ψ and θ angles are not orthogonal, as was the case in compounds **1**–**5** and **7**, but slightly smaller as a function of non-linearity of the Hg(1)–N(1)–C(2) line, which in turn

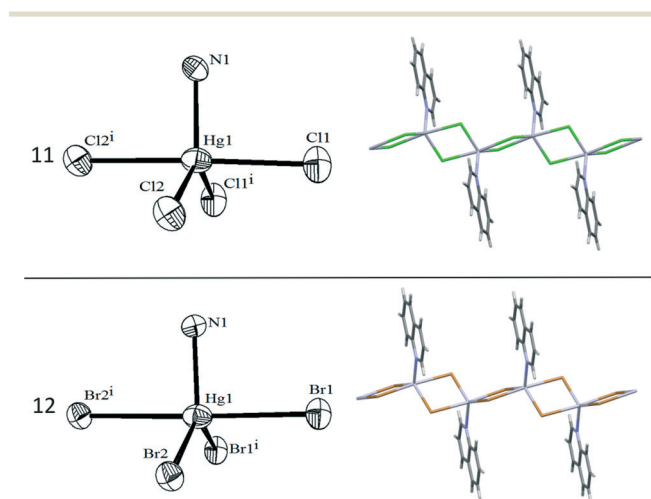


Fig. 16 (left) Five-coordinate Hg²⁺ metal centres of **11** and **12**, showing the numbering scheme of symmetry-generated halide ligands. (right) Section of the one-dimensional halide-bridged polymers of **11** and **12**, viewed perpendicular to the direction of chain propagation. Symmetry transformation used to generate equivalent atoms: ⁱ–x, –y, –z.

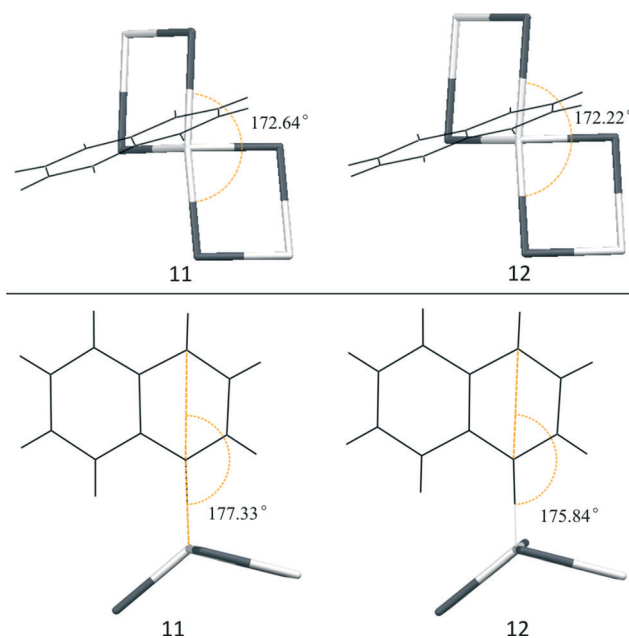


Fig. 17 Curving of the axial X(1)–Hg–X(2) line in compounds **11** (left) and **12** (right) away from the benzo-part of the quinoline ligand (top). Curving of the Hg(1)–N(1)–C(2) line in compounds **11** (left) and **12** (right), as viewed along the direction of chain propagation (bottom).

results from the asymmetric nature of the quinoline ligand. Weak interchain *meta*-C–H $\cdots\mu$ -X–M hydrogen bonding interactions between the H(2) atoms of the C(2) ring carbons and the bridging X(1) halide anions of the smaller ribbon loops in the neighbouring chain result in the structure forming a two-dimensional hydrogen-bonded sheet parallel to the *bc*-plane, as shown in Fig. 19(b).

Hydrogen bonding parameters are listed in Table 8. The packing arrangement of **11** and **12**, as illustrated in Fig. 20, is layered and forms alternating organic and inorganic monolayers parallel to the *ac*-plane. Aromatic interactions zipper together neighbouring one-dimensional chains in the *c*-direction. The resulting interdigitation between the quinoline ligands in the organic layer is illustrated in Fig. 20. Since the quinoline ligand is slightly puckered, with a total puckering amplitude (*Q*) (ref. 23) of 0.06(2) $^\circ$ in **11** and 0.022(10) $^\circ$ in **12**, all the smallest centroid-to-centroid distances are between interdigitated six-membered aromatic ring planes that are not parallel as reflected in the non-zero α angles collated in Table 9. The asymmetry of the ligand system, together with the alternating position and opposite orientation of the organic ligand on different sides of the polymer chain, results in the positioning of the nitrogen atoms on the zipped organic ligands to be optimally slipped relative to each other. Due to the asymmetry of the bridging unit, two alternating centroid-to-centroid interactions are observed. All ring interaction parameters of **11** and **12** are listed in Table 9.

[Hg₂(μ -I)₂I₂(quin)₂] (**13**) and [Hg₂(μ -I)₂I₂(acr)₂] (**6**)

The only two iodide members in the family of compounds studied, **6** and **13**, were found to exhibit similar crystal structures. The organic ligand-to-metal halide ratio of 1:1 which was employed in the synthesis is reflected in the crystal structures. The asymmetric units of **6** and **13** consist of a tetrahedral Hg²⁺ ion coordinated to two iodide ligands and one quinoline or one acridine ligand, respectively, *via* the nitrogen atom, as illustrated in Fig. 1. Two asymmetric units comprise each unit cell with none of the atoms occupying special positions. The full repeat unit is generated by operation of an inversion centre on the asymmetric unit, as illustrated in Fig. 21 (right). Compounds **6** and **13** both crystallise in the triclinic space group *P* $\bar{1}$, and their crystallographic parameters are listed in Table 2.

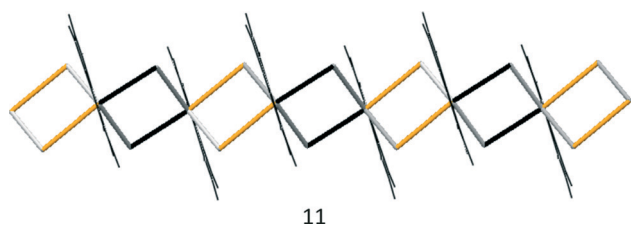


Fig. 18 Section of the one-dimensional halide-bridged polymer of **11**, with the larger bond distances in each loop highlighted in black for the smaller loops and orange for the larger loops.

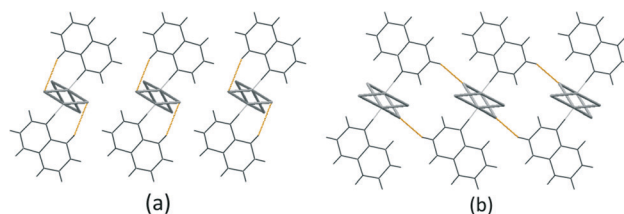


Fig. 19 (a) Weak intrachain C–H $\cdots\mu$ -X–M hydrogen bonding in **11** as viewed down the crystallographic *a*-axis. (b) Weak interchain *meta*-C–H $\cdots\mu$ -X–M hydrogen bonding between adjacent chains of **12** as viewed down the crystallographic *a*-axis.

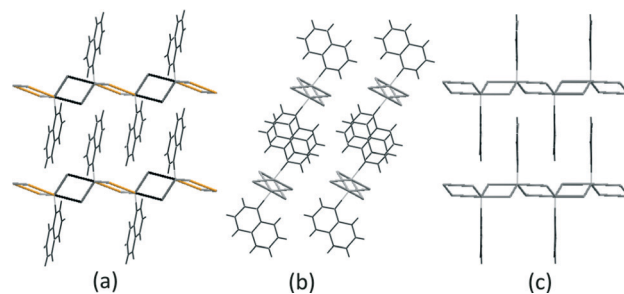


Fig. 20 (a) Packing arrangement of **11** as viewed down the crystallographic *b*-axis. (b) Packing arrangement of **12** as viewed down the crystallographic *a*-axis. (c) Packing arrangement of **11** as viewed along the mean plane of the quinoline ligands.

In both **6** and **13**, the Hg²⁺ metal centre adopts a tetrahedral coordination geometry. The I(2) halide ligand and its symmetry-generated counterpart act as bridging ligands and connect two adjacent Hg²⁺ metal centres as edge-sharing tetrahedra to form zero-dimensional double halide-bridged dimers, as shown in Fig. 21 (right). The two bridging iodide ligands together with one terminal iodido ligand and the nitrogen atom of quinoline in **13** and acridine in **6** satisfy the geometric requirements of the four-coordinate metal centre, as illustrated in Fig. 21 (left). Selected bond lengths and angles are given in Table 6.

Even though complexes **6** and **13** can be considered as zero-dimensional, isolated dimers, stacking of the dimeric units occurs in both **6** and **13** along the *b*-direction, as illustrated in Fig. 22, aligning the dimers in a chain-like fashion. The inter-dimer M \cdots X (Å) and M(1) \cdots M(1) (Å) distances are collated in Table 6 and can be seen to increase from compound **6** to **13** with an increase in size of the N-donor ligand. The inter-unit M(1) \cdots M(3) distance along the pseudo-chain is equal to the *b* cell spacing. The *b*-axis is, however, not the shortest lattice parameter in compounds **6** and **13**; the *a*-axis is. Both of the pseudo-chains adopt a zigzag ribbon motif, as seen in compounds **1**–**5** and **7** as well as **11** and **12**, with the coordinated organic ligands alternating between the ‘above’ and ‘below’ positions on successive metal centres as well as between sides to which the asymmetric ligand protrudes when viewed perpendicular to the direction of chain propagation.

The coordination number of the metal centre in the pseudo-chain is five, and the coordination geometry of the

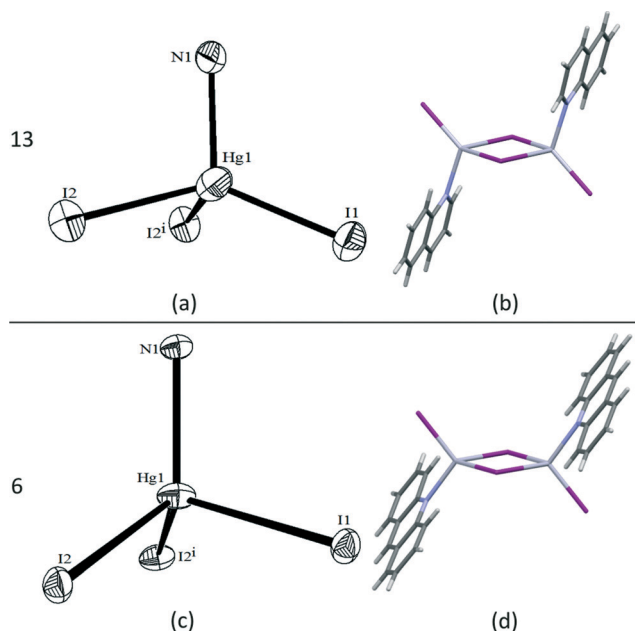


Fig. 21 (a, c) Four-coordinate Hg^{2+} metal centres of **6** and **13**, showing the numbering scheme of the symmetry-generated iodide ligand. (b, d) Halide-bridged dimers of **6** and **13**. Symmetry transformation used to generate equivalent atoms: $^i-x, -y, -z$.

Table 6 Selected bond distances and angles in **6** and **13** (\AA , $^\circ$), M = Hg, X = I

	13	6
Terminal M–X (\AA)	2.625(1)	2.6739(5)
Bridging M–X (\AA)	3.068(1), 2.756(1)	2.8885(4), 2.8422(3)
M–N (\AA)	2.32(1)	2.331(4)
Bridging X–M–X ($^\circ$)	92.56(4)	90.13(1)
Terminal X–M–X ($^\circ$)	133.63(4), 104.32(4)	118.02(1), 113.31(1)
Terminal X–M–N ($^\circ$)	115.5(3)	107.5(1)
Bridging X–M–N ($^\circ$)	104.2(3), 97.7(3)	107.4(1), 120.0(1)
M–X–M ($^\circ$)	87.44(3)	89.87(1)
M(1)⋯M(2) (\AA)	4.0318(9)	4.0478(3)
ψ ($^\circ$)	81.3(3)	84.5(1)
θ ($^\circ$)	78.7(5)	81.8(1)
ω ($^\circ$)	54(1)	128.6(4)
Inter-dimer M⋯X (\AA)	4.252(2)	5.1130(4)
Inter-dimer M(1)⋯M(1) (\AA)	5.564(1)	6.7241(4)
Inter-dimer M(1)⋯M(3) (\AA)	8.770(1)	9.1306(5)

metal ion is distorted square pyramidal. Fig. 22 shows a section of the pseudo-chains in both compounds with the inter-dimer $\text{Hg}(1)\cdots\text{I}(2)$ contacts indicated in orange.

None of the M–X distances in the pseudo-chains, in either **6** or **13**, are equidistant. The side lengths of the parallelogram bridging unit in **13** differ substantially. This is not the case in **6**, in which the bridging unit approaches a perfectly

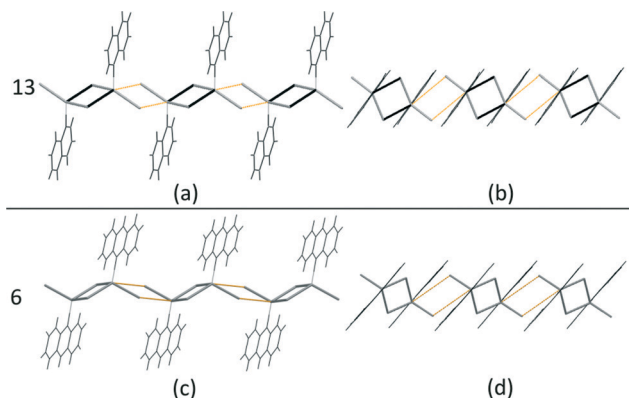


Fig. 22 (a, c) Inter-dimer contacts between dimeric units of **12** and **13** as viewed perpendicular to the direction of chain propagation. (b, d) Inter-dimer contacts between dimeric units of **12** and **13** as viewed down the crystallographic c -axis. In compound **12**, the larger bond distances in each bridging loop are highlighted in black with the inter-dimer contacts in orange in both pictures.

square geometry. The difference between the bridging units in **6** and **13** is a result of both preformed HgX_2 -unit remnants and the structural differences in the coordinated N-donor organic ligands. The tetrahedral environment surrounding the Hg^{2+} metal centre in **13** accommodates the asymmetric nature of the N-donor ligand with its concomitant difference in the steric requirement on different sides of the halide-bridged dimer by increasing the $\angle(\text{I}(1)\text{--Hg}(1)\text{--I}(2))$ angle to $133.63(4)^\circ$ on the side to which the benzo-part of the ligand is positioned and decreasing the $\angle(\text{I}(1)\text{--Hg}(1)\text{--I}(2))$ angle to $104.32(4)^\circ$ on the other side. Due to the symmetric nature of the acridine ligand in **6**, the corresponding angles are $118.02(1)^\circ$ and $113.31(1)^\circ$, respectively.

The intra-dimer conformation is described by the same parameters (ψ , θ and ω) used for describing the intrachain conformations of the polymers and is schematically illustrated in Scheme 1. Note, however, that the measurements were not made on the isolated dimers, but by treating the repeating dimers as a pseudo-one-dimensional chain, as explained earlier. Weak intrachain $\text{C--H}\cdots\mu\text{--X--M}$ hydrogen contacts are present in **13** between the $\text{C}(1)\text{--H}(1)$ functionality of the quinoline ligand and the bridging halide ligands of the respective dimer, and although the distance of 3.290\AA is too large for the contacts to be considered as formal hydrogen bonds, as defined in Mercury,¹⁸ the orientation of the ligand relative to the pseudo-chain suggests that the intrachain $\text{C--H}\cdots\mu\text{--X--M}$ interactions contribute to the observed ω angle of $54(1)^\circ$, as illustrated in Fig. 23. Weak, stabilising inter-dimer $\text{C--H}\cdots\text{X--M}$ hydrogen contacts between the $\text{H}(8)$ atoms on the $\text{C}(8)$ ring carbons and the terminal $\text{I}(1)$ halido ligands in neighbouring dimers in the b -direction assist in maintaining the structural integrity of the pseudo-one-dimensional chain in compound **13**, as shown in Fig. 23 (top).

In compound **6**, weak intrachain $\text{C--H}\cdots\mu\text{--X--M}$ hydrogen contacts are present between the $\text{H}(1)$ and $\text{H}(12)$ atoms of

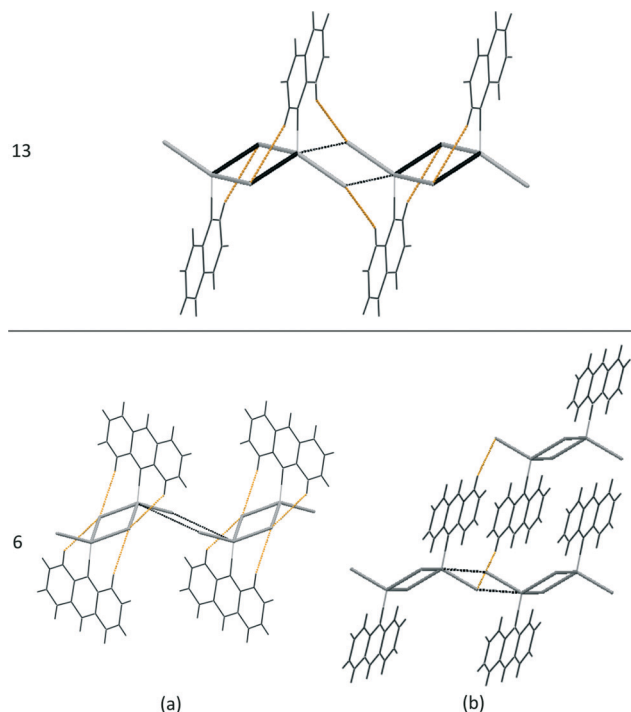


Fig. 23 Intrachain C-H...μ-X-M hydrogen contacts in **13** (top). (a) Intrachain C-H...μ-X-M hydrogen contacts in **6**. (b) Interchain C-H...μ-X-M hydrogen contacts between neighbouring pseudo-chains in **6**. Contacts between adjacent dimers, forming the pseudo-chains, are indicated in black.

the C(1) and C(12) atoms of the acridine ligands and the two bridging halide ligands of the dimer, respectively, as illustrated in Fig. 23(a), again contributing to the observed ω angle of $128.6(4)^\circ$. Interchain C-H...μ-X-M hydrogen bonding interactions between the H(9) atoms on the C(9) ring carbons and the bridging iodide ligands in a neighbouring pseudo-chain are also shown in Fig. 23. The ψ and θ angles are not orthogonal in either **6** or **13**, but smaller as a result of the tetrahedral nature of the Hg^{2+} metal centres. Short hydrogen contact parameters are listed in Table 8.

The packing arrangement in both of the compounds is layered, alternating between organic and inorganic monolayers parallel to the bc -plane. When viewed down the crystallographic a -axis, the extent of interdigitation between the N-donor ligands between neighbouring dimers can be seen, as illustrated in Fig. 24(a-d). This interdigitation allows for the formation of aromatic interactions between aromatic rings. The ring interaction parameters of **6** and **13** are listed in Table 9. As was observed in compounds **11** and **12**, the quinoline ligands are slightly puckered with $Q = 0.026(17)^\circ$. As expected, the centroid-to-centroid distances alternate in both compounds with the alternating size of the intra- and inter-dimer bridging units. The shortest centroid-to-centroid distances in **13** are, however, between parallel constituent aromatic rings, with small perpendicular slippage distances indicating an almost perfect head-to-tail alignment; the asymmetric nature of the organic ligands together with their head-

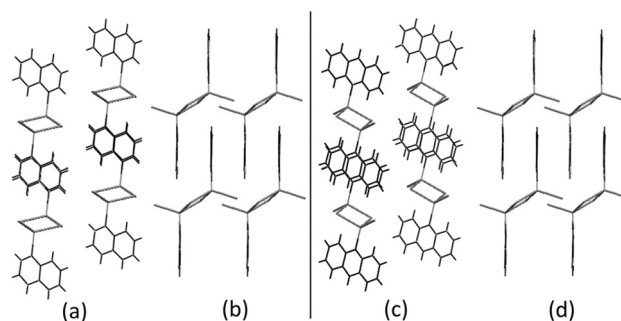


Fig. 24 (a, c) Packing arrangement of the pseudo-chains of **6** and **13** as viewed down the crystallographic b -axis. (b, d) Packing arrangement of **6** and **13** as viewed along the mean plane of the coordinated organic ligands.

to-tail orientation is such that the nitrogen atoms are on opposite sides of the respective ring systems. Head-to-tail stacking is also observed between the acridine moieties contained in **6**. However, since the acridine ligands in **6** are planar and parallel, the centroid-to-centroid distances can be measured between the centroids of the N-containing rings, as was the case in all the other acridine ligand-containing compounds.

Since the centroid-to-centroid distances between the organic ligands in compounds **6** and **13** are comparable with those found in compounds **1–5** and **7–12**, the primary contact adhesive responsible for the pseudo-chain integrity seems to be the aromatic zipper interactions between the organic ligands, rather than the, albeit contributing, long-range interdimer $\text{M}\cdots\text{X}$ interactions. The alternating disruption in the halide-bridged scaffold, induced by the sheer bulk of the constituent ions, provides the steric freedom required by the aromatic moieties to achieve the degree of interdigitation needed to keep the pseudo-chain intact.

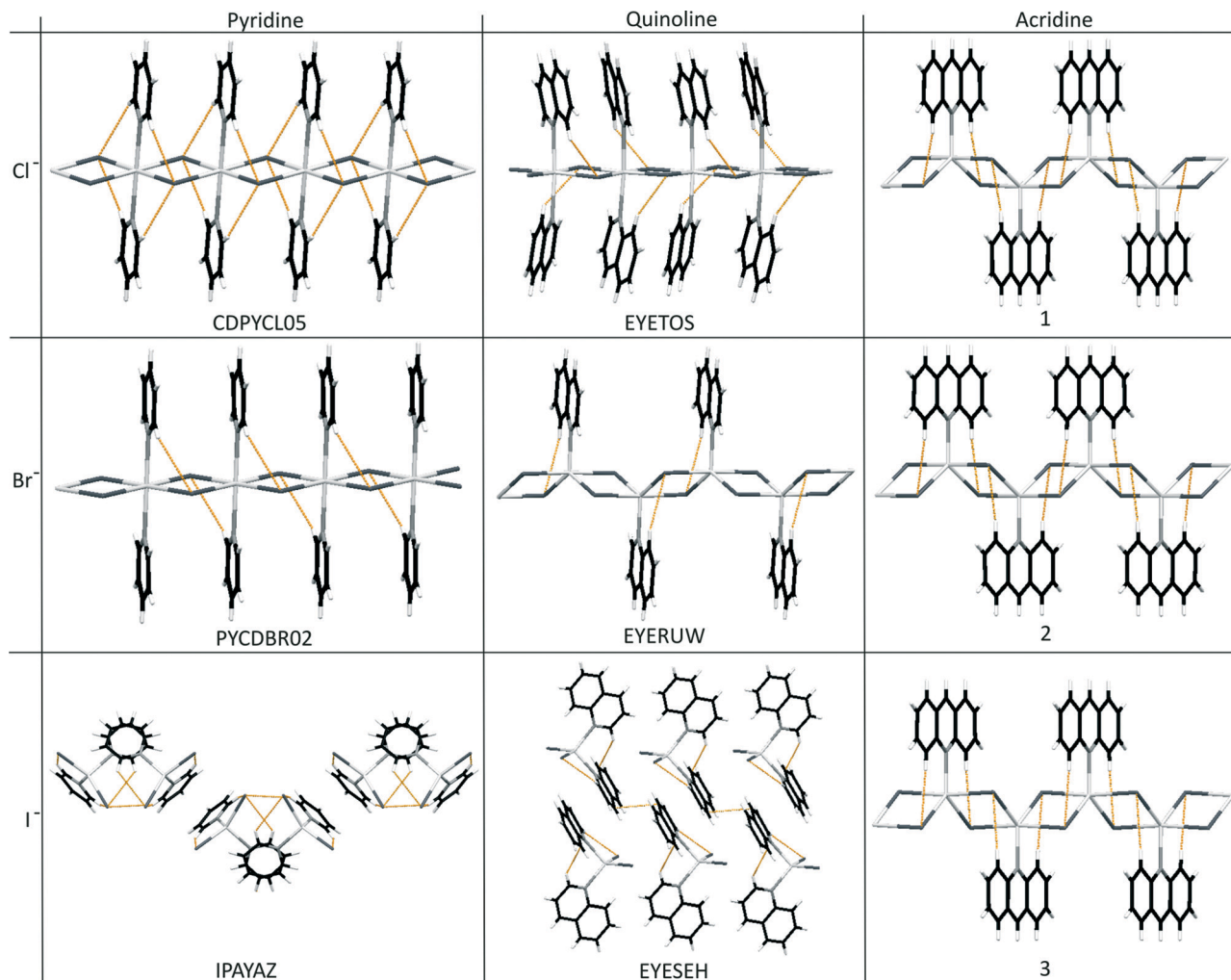
Overall comparison

Novel structures **1–13** can now be compared to related structures reported in the literature in order to investigate the effect of increasing the width of the N-donor ligand in one dimension on halide-bridged chain attributes. Included in the comparison are structures containing the organic ligands pyridine, which consists of one aromatic ring, quinoline, which comprises two aromatic rings, and acridine, which consists of three aromatic rings, with the N-donor atom in similar relative positions.

Six divalent cadmium compounds with pyridine and quinoline as organic N-donor ligands and three Hg^{2+} -containing compounds with pyridine as the organic ligand were mined from the CSD¹⁵ and are presented together with the novel structures **1–13** in Schemes 3 and 4.

Cadmium structures

The combination of the literature results with structures **1–3** from the current study provides a matrix of Cd^{2+} compounds



Scheme 3 Sections of the one-dimensional linear chains and zero-dimensional molecular compounds with progression related to both the width of the N-donor ligands and the size of the halide ligands. Hydrogen bonds, hydrogen contacts and selected short contacts are indicated in orange. Structural results from ref. 6, 14, 24.

in which the organic ligand spans a range of widths, as summarized in Scheme 3. CDPYCL05,²⁴ PYCDBR01–02 (ref. 6 and 24) and IPAYAZ⁶ all contain Cd²⁺ as the metal cation with pyridine as the coordinated N-donor ligand and chloride, bromide and iodide as the halide ligands, respectively. CDPYCL05 and PYCDBR02 are isostructural and both crystallise in the monoclinic space group $P2_1/n$, while PYCDBR01 and IPAYAZ crystallise in the orthorhombic space groups, $Pnmm$ and $Pbca$, respectively. Both bromide polymorphs²⁴ exist as halide-bridged polymers, with a thermotropic polymorphic phase transition occurring at *ca.* 175 K. In the chloride and bromide compounds, the cationic metal nodes are six-coordinate, with the N-donor pyridine ligands coordinated *trans* to each other in the axial positions of the cation's coordination sphere and the four halide ligands equatorially coordinated. *Trans* edge-sharing between adjacent octahedra results in the observed one-dimensional halide-bridged chains. Aromatic interactions are present between the aromatic moieties coordinated to adjacent metal centres. The

iodide compound IPAYAZ crystallises in the orthorhombic space group $Pbca$. The cationic metal centres in IPAYAZ adopt a tetrahedral coordination geometry and are coordinated to two N-donor pyridine ligands and two iodido ligands. The compound is zero-dimensional and the chain integrity, as observed in CDPYCL05 and PYCDBR01–02, is lost in IPAYAZ through the sheer bulk of the constituent inorganic ions together with the small aromatic surfaces provided by the coordinated pyridine N-donor ligands. Intermolecular association between the aromatic moieties does, however, include both face-to-face and point-to-face arrangements.^{20,25} No Cd–I⋯Cd–I close contacts are observed in the structure. The compounds EYETOS, EYERUW and EYSEH were all synthesised and structurally characterised by Bowmaker *et al.*¹⁴ The said compounds all contain Cd²⁺ as the cationic metal centre and quinoline as the coordinated N-donor ligand, but differ with regard to the coordinated halide ligands, which are chloride, bromide and iodide, respectively. EYETOS crystallises in the orthorhombic space group $P42_1c$.

The Cd²⁺ metal centre adopts an octahedral geometry with two N-donor ligands coordinated *trans* to each other in the axial positions of the said sphere, while the four chloride ligands coordinate in the equatorial plane and partake in edge-sharing to connect the adjacent octahedra into a one-dimensional halide-bridged chain. The asymmetric nature of the quinoline ligand is accommodated in various ways by the system: firstly, the benzo-part of the quinoline ligands alternates in sides to which it protrudes relative to the halide-bridged chain. Secondly, the ligand is tilted in such a way as to project the benzo-part of the ligand away from the halide-bridged chain in order to relieve steric tension between the C(8)–H(8) functionality of the benzo-ring and the bridging chloride ligands and allow weak intrachain C(8)–H(8)⋯μ-Cl–Cd hydrogen bonding. The halide-bridged chain in EYETOS also accommodates the additional steric effects introduced by the benzo-part of the ligand by tilting the bridging unit in such a way that the participating μ-Cl ligand moves downwards, away from the C(8)–H(8) functionality, thereby preserving the weak intrachain C(8)–H(8)⋯μ-Cl–Cd hydrogen bonding interaction. This results in the mean planes through the ions comprising adjacent bridging units of the halide-bridged chain not being coplanar, as was the case in CDPYCL05, but to be slightly tilted relative to each other at an angle of 3.56°. Both of the said adjustments also disrupt the weak intrachain *ortho*-C(1)–H(1)⋯μ-Cl–Cd hydrogen bonding interactions on the pyridine side of the ligand that were observed in CDPYCL05 shown in Scheme 3 by reducing the ∠(DHA) angle to a value that is not conducive to hydrogen bonding, as can be seen in Scheme 3. In addition, neighbouring organic N-donor ligands on the same sides of the halide-bridged chain are not parallel, but rotated in plane relative to each other. The centroid-to-centroid distances are, however, at 3.802 Å, still indicative of aromatic interactions between the neighbouring aromatic moieties.

The quinoline compound EYERUW has the larger bridging bromide ligand incorporated into the halide-bridged chain. The Cd²⁺ metal cation has to scale down on the number of coordinating ligands, due to the increased steric demand of the bromide ligand, to preserve chain integrity, and the coordination number reduces to five. The compound crystallises in the triclinic space group *P* $\bar{1}$. The five-coordinate metal centre now adopts a trigonal bipyramidal coordination geometry, and the chain conformation changes from the flat ribbon, as observed in CDPYCL05, PYCDBR01–02 and EYETOS, to a zigzag ribbon, as illustrated schematically in Scheme 2.

This has the effect of bringing the metal centres closer together, relative to what would be the case in an equivalent flat polymer. Since the organic ligands alternate on opposite sides of the polymer, the zigzag ribbon conformation also allows for tailoring of the distance between organic ligands to permit the interdigitation of organic ligands from neighbouring chains, which is not possible in the case of the flat polymers since the organic ligands fill all sites above and below the polymer chain. The importance of aromatic interactions as a supramolecular motif becomes evident in the

iodide analogue of this series, EYSEH. EYSEH crystallises in the triclinic space group *P* $\bar{1}$ with the Cd²⁺ metal in a tetrahedral geometry. The four-coordinate metal cation is coordinated to two iodido ligands and two N-donor quinoline ligands. The sheer bulk of the constituent inorganic ions results in the compound being zero-dimensional. In comparison to the pyridine ligand in IPAYAZ, the larger aromatic surface provided by the quinoline ligand in EYERUW now makes association of the aromatic quinoline ligands energetically favourable, forming a definite organic layer in which the quinoline ligands are stacked. This arrangement then also aligns the inorganic components of the molecular repeat units, which was not the case in IPAYAZ; however, the Cd–I⋯Cd contacts are still too long for the structure to be considered a pseudo-polymer as in 6 and 13.

Adaptation of the weak intrachain C–H⋯μ-Cl–Cd hydrogen bonding interactions and the change in chain conformation with increasing width of the N-donor ligand from pyridine to quinoline to acridine, as well as the effect thereof on the halide-bridged chain geometry in the cadmium family of compounds were next considered. The pyridine chloride and bromide members of this family, CDPYCL05 and PYCDBR02, adopt a flat ribbon chain motif. The hydrogen bonding interactions in these compounds were discussed in detail in a recent review.¹¹ In the chloride members of the cadmium family, the organic ligand changes from pyridine in CDPYCL05 to quinoline in EYETOS and acridine in compound 1. The weak hydrogen intrachain C–H⋯μ-Cl–Cd hydrogen bonding in these structures is visually presented in Scheme 3. To reiterate what was observed in the pyridine and quinoline chloride analogues and including compound 1 in the discussion, ring tilting and rotation in EYETOS disrupt the weak intrachain *ortho*-C(1)–H(1)⋯μ-Cl–Cd hydrogen bonding interactions on the pyridine side of the ligand, as was observed in CDPYCL05 and is shown in Scheme 3, by reducing the ∠(DHA) angle to a value that is not conducive to hydrogen bonding. Considering acridine chloride analogue 1, both the zigzag chain motif and the rotation of the acridine ligands about the M–N axis promote the establishment of stabilising C(2)–H(2)⋯μ-Cl–Cd hydrogen bonds on both sides of the halide-bridged chain, as illustrated in Scheme 3. The zigzag ribbon conformation observed in compound 1 much better accommodates the steric effects introduced by the benzo-parts of the acridine ligand, by having two of the bridging chloride ligands form two of the three legs of the resulting trigonal plane and thus pointing away from the C(2)–H(2) organic ring functionalities in compound 1.

In the bromide series of the Cd²⁺ compounds, the width of the ligand increases along the series PYCDBR01–02, EYERUW and 2. While the pyridine member of the series, PYCDBR01–02, shows a coordination number of six and a flat ribbon motif, EYERUW, which contains a quinoline ligand, breaks the pattern and adopts a zigzag ribbon motif, with a coordination number of five, which can be explained by applying the same reasoning as that used to explain the change in chain conformation between EYETOS and 1 in the

preceding text. The N-donor quinoline ligands in EYERUW are now arranged in a slip-one-knit-one fashion along the halide-bridged chain, and intrachain aromatic interactions are lost. Interchain aromatic interactions are, however, introduced in this arrangement *via* interdigitation of the aromatic moieties of adjacent chains, as was the case in **1**. This molecular zipper arrangement now involves aromatic–aromatic interactions in which the heteroatoms do not overlap, as was the case in EYETOS, and in which the participating aromatic organic moieties are parallel with the closest centroid-to-centroid distance of 3.642 Å. The twist in the zigzag ribbon motif then also serves to conserve aromatic–aromatic interactions between the coordinated organic moieties, in that it creates an opening for the interdigitation of organic moieties from adjacent chains. The size of the bridging unit or the M(1)⋯M(2) distance dictates the centroid-to-centroid distances observed between the coordinated aromatic moieties in the six-coordinate systems, and although rotation around the M–N bond may achieve parallel slipped arrangements conducive to aromatic–aromatic interactions in these systems, this rotation can also only stretch so far until the aromatic interactions are disrupted. The zigzag ribbon motif introduces a means to conserve these non-covalent aromatic interactions, albeit interchain aromatic–aromatic interactions, between interdigitated aromatic moieties. Upon consideration of the iodide Cd²⁺-containing series, the pyridine-containing compound IPAYAZ displays a pyridine-to-metal halide ratio of 2:1 and is zero-dimensional, and the chain integrity, as observed in its chloride and bromide congeners, CDPYCL05 and PYCDBR01–02, is lost in IPAYAZ, as explained earlier.

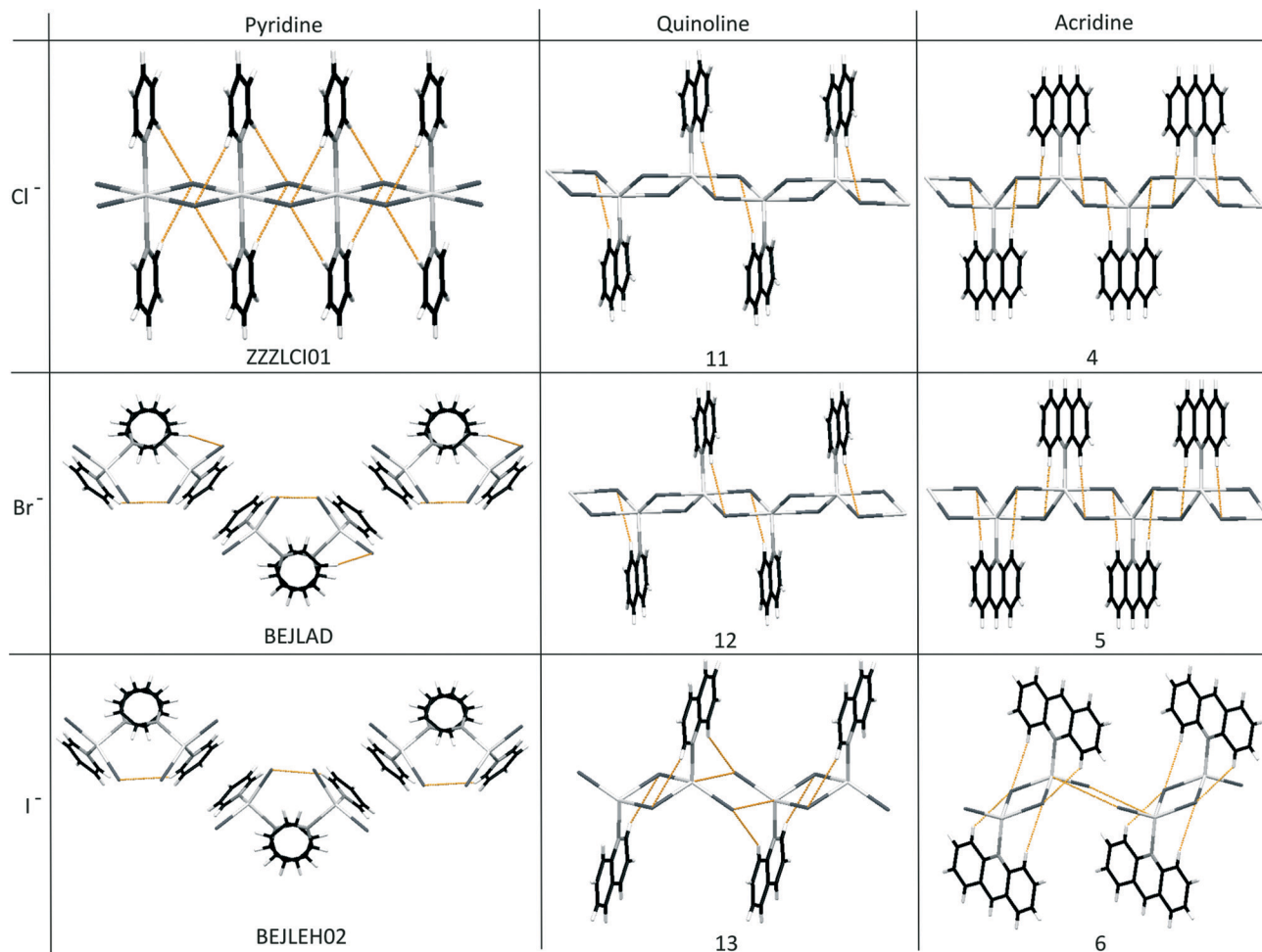
Moving to the quinoline analogue, EYSEH, and as stated in the preceding text, the larger aromatic surface induced by the coordinated N-donor ligand, quinoline, provides the energetic incentive for the aromatic quinoline ligands to associate and thereby form a definite stacked organic layer, with concomitant alignment of the inorganic components present in the repeat unit of the compound.

Moving across the series to compound **3**, the coordination number of the Cd²⁺ metal centre increases from four-coordinate to five-coordinate, trigonal bipyramidal coordination, with the polymeric chain in the zigzag ribbon conformation as observed in EYERUW, **1** and **2**. As stated previously, this has the effect of bringing the metal centres closer together, but here, the driving force seems to be the stability gained by aromatic interactions *via* interdigitation of the larger aromatic moieties of neighbouring chains.

Mercury compounds

Considering the Hg²⁺ compounds, Scheme 4 depicts the change in chain configuration or chain integrity, with increasing width of the N-donor ligand and increasing size of the halide ligand in the Hg²⁺ family of pyridine, quinoline and acridine compounds. Discussion of compounds **4–6** and **11–13** can be found in the preceding text and will not be

repeated here, but the structures will be compared here to the related structures reported in the literature, giving a full matrix of compounds with Hg²⁺ as the cationic metal centre. The compounds in Scheme 4 which contain pyridine as the N-donor ligand were all deposited by the same authors, Canty *et al.*,²⁶ in an effort to clarify the reputed polymeric structure of the chloride analogue and the monomeric structures of the bromido and iodido analogues. ZZZLCI01,²⁶ the pyridine chloride analogue, is indeed polymeric and crystallises in the monoclinic space group *P*₂₁/*n*. The metal nodes comprise six-coordinate Hg²⁺ cations, coordinated to two N-donor pyridine ligands in the axial positions and four chloride ligands in the equatorial plane of each of the said octahedra. Chain propagation occurs *via* a *trans* edge-shared connectivity pattern of the adjacent octahedra. The bromido and iodido analogues, BEJLAD²⁶ and BEJLEH,²⁶ crystallise in the orthorhombic space groups, *Pca*2₁ and *Pnma*, respectively, and form zero-dimensional tetrahedral complexes instead of a halide-bridge polymer. A second zero-dimensional polymorph of BEJLEH is also known, BEJLEH02,²⁷ in which the orthorhombic space group settings are slightly modified to *Pbca* wherein the packing of the molecules is different. Note that the pyridine-to-metal halide ratio is 1:2 in both the polymeric structure ZZZLCI01 and the zero-dimensional structures BEJLAD and BEJLEH01–02. In the zero-dimensional, tetrahedral bromido and iodido analogues, the metal cation is coordinated to two halido ligands and two N-donor pyridine ligands in each instance. No Hg⋯X contacts that may hint at the formation of a pseudo-halide-bridged chain are observed in any of the zero-dimensional pyridine structures. Thus, taking the pyridine series of Hg²⁺ into consideration, chain disruption is evident in the bromido- and iodido-containing analogues and can be ascribed to the sheer bulk of the constituent inorganic ions. The aromatic surfaces provided by the pyridine ligands are not large enough to energetically promote the zippered arrangement between the aromatic moieties required to form a pseudo-chain or chain in these compounds, and only pairwise association between the said moieties is observed. In summary, in the chloride series of the Hg²⁺ compounds, the coordination number of the metal centre decreases with increasing width of the coordinating N-donor ligand. With pyridine as the coordinating N-donor ligand, the Hg²⁺ metal centre is six-coordinate, while the coordination number reduces to five with both quinoline and acridine as N-donor ligands. In the bromide series of the Hg²⁺ compounds, chain integrity remains intact in compounds **12** and **5**, which has quinoline and acridine as N-donor ligands, respectively, due to reasons explained in the preceding text. In the pyridine counterpart of the bromide series, the Hg²⁺ metal centre displays a tetrahedral coordination geometry. In the iodide series of the Hg²⁺ compounds, the pyridine member of the series displays a tetrahedral coordination geometry. The quinoline and acridine members of the series, compounds **6** and **13**, form five-coordinate pseudo-polymer chains due to the larger size of the inorganic components comprising the system.



Scheme 4 Sections of the one-dimensional linear chains and zero-dimensional molecular compounds with progression related to both the width of the N-donor ligands and the size of the halide ligands in the Hg^{2+} family of compounds. Hydrogen bonds, hydrogen contacts and selected short contacts are indicated in orange. Structural results from ref. 26.

Conclusion

The geometric preferences and concomitant coordination geometries of metal ions, bestowed by their oxidation state, are two of the fundamental aspects of coordination chemistry.²⁸ The electronic geometries adopted by the metal ions presented in the current study, however, highlight the important templating effect contributed by the organic donor ligand. The eleven novel one-dimensional halide-bridged polymers (1–5 and 7–12) and two pseudo-chains (6 and 13) reported in this study robustly grouped themselves into two different structural types based on the coordination geometry adopted by the metal cation. Compound 10 is the only compound which displays a 1:2 ratio of organic ligand to metal halide, and is therefore not considered in trend formulation. In compounds 1–5 and 7–12, the metal centres are all penta-coordinate M^{2+} cations which include both Cd^{2+} and Hg^{2+} . The coordination geometry adopted by the Cd^{2+} cations is restricted to trigonal bipyramidal with both acridine and phenazine as N-donor organic ligands (compounds 1–3 and 7). The five-coordinate Cd^{2+} metal centres are linked *via*

edge-sharing of adjacent pentahedra resulting in the observed zigzag ribbon conformation, as illustrated in Scheme 2. The structural integrity of the one-dimensional halide-bridged chains, with Cd^{2+} as the metal centre, is conserved with the increase in size of the bridging halide ligand, except for the two pyridine iodide analogues. Hg^{2+} as the cationic metal centre adopts a variety of coordination geometries, depending on the topology of the organic N-donor ligand and the size of the bridging halide ligand. All mercuric polyhedra do, however, connect *via* edge-sharing to form one-dimensional chains of zigzag ribbon conformation, excluding the pyridine bromide and iodide analogues. With iodide and certain bromides as bridging halide ligands, the structural integrity of the halide-bridged chain is lost due to the sheer bulk of the constituent inorganic ions, although remnants of the one-dimensional halide-bridged chain persist as stacked dimers which exhibit long, semi-coordinate bonds forming pseudo-chains. With chloride and bromide as bridging halide ligands, the chain remains intact, except for the pyridine bromide analogues. Bridged by chloride and bromide ligands, the Hg^{2+} cation adopts a trigonal bipyramidal coordination

geometry with the monotopic N-donor organic ligands, acridine and quinoline, with the chain conformation very close to that observed in its Cd^{2+} counterparts. A square pyramidal coordination geometry is however adopted by the Hg^{2+} cation when the N-donor organic ligand is ditopic. This effect is a function of the natural affinity of Hg^{2+} for ligating nitrogen atoms, as reflected in the short Hg–N bond distances collated. The coordination geometry adopted by the Hg^{2+} cation can therefore also be argued to be pseudo-octahedral, with the long-range, semi-coordinative interactions with the second nitrogen atom of the phenazine ligand occupying the sixth position of the said octahedron. Table 7 provides a summary of the coordination geometries adopted by Cd^{2+} and Hg^{2+} with the increase in size of the bridging halide ligand and the increase in width of the N-donor ligand.

The descriptors ψ , θ and ω , as introduced by Englert *et al.*⁶ for the description of the intrachain conformations of the halide-bridged chains coordinated by N-donor organic ligands, were also invoked in this contribution as an aid to classify structural types. All the halide-bridged polymers in this contribution that crystallise in the monoclinic space group $C2/c$ (1–5 and 7) have ψ and θ angles that approximate 90° . The ω angle in the $C2/c$ polymers is not orthogonal to the $M\cdots M$ vector and decreases with an increase in size of the bridging halide ligands. The $C2/c$ space group setting was found to apply to both Cd^{2+} and Hg^{2+} as nodal cations. All but one $C2/c$ halide-bridged chain contain acridine as the coordinated N-donor ligand. Compound 7, however, contains phenazine as the coordinated organic ligand, but since the nodal cation is Cd^{2+} , the symmetry is not lost as is the case observed in Hg^{2+} nodes with ditopic N-donor ligands, as discussed earlier. None of the descriptors approximate orthogonality in any of the $P\bar{1}$ chains. The loss of symmetry is then also evident from the triclinic space group assignment. In compounds 8 and 9, which contain Hg^{2+} cations as metal nodes with phenazine as the coordinated N-donor ligand, the natural affinity of Hg^{2+} for N-donor ligands is evident from the long-range interactions observed between the second nitrogen atom of the phenazine ligands and the metal cation in adjacent chains. The adjacent chains are, however, slipped relative to each other and the long-range interactions are possible by adjustment of both the ψ and θ angles. In compounds 11 and 12, where the chains comprise Hg^{2+} metal cations that are coordinated by the monotopic N-donor ligand, quinoline, the symmetry is lost due to the asymmetric nature of the coordinated N-donor organic ligand and concomitant deformation of the halide-bridged chain is observed.

The important stabilising role of various secondary non-covalent interactions becomes apparent in this contribution. Both weak intra- and interchain C–H \cdots μ -X–M interactions are present in all compounds, with the interchain C–H \cdots μ -X–M interactions resulting in the formation of extended 2D hydrogen-bonded frameworks. The slip-one-knit-one arrangement of the N-donor ligands along the polymeric chains, as a function of ligand size and topicity of the N-donor ligands,

allows organic moieties from adjacent chains to interdigitate and effectively fill the ‘slipped’ positions in neighbouring chains.

Interdigitation is directed by both interchain C–H \cdots μ -X–M interactions and aromatic interactions between the organic moieties. These aromatic zipper interactions emerge as a supramolecular bonding motif and are observed in compounds 1–9 and 11–13. In compounds 1–5, 7–9, 11 and 12, interdigitation of the aromatic moieties may be argued to be a function of close packing. In compounds 6 and 13, however, where the steric bulk of the halide-bridged chain composites is such that chain integrity cannot be maintained by coordinative bonding, the importance of these interactions, together with interchain C–H \cdots μ -X–M interactions, in maintaining the chain integrity becomes evident. The question posed in the introduction regarding the effects of the increase in size of the halide ligand, from chloride to iodide, together with the increase in size of the chosen N-donor ligand type, on chain integrity has been addressed.

Experimental

Chemicals and reagents

All chemicals were used as-purchased without further purification: HgCl_2 (98%, Fluka), HgBr_2 (98%, Sigma Aldrich), HgI_2 (99%, Riedel de Haen), $\text{CdCl}_2\cdot 2.5\text{H}_2\text{O}$ (99%, Riedel de Haen), $\text{CdBr}_2\cdot 4\text{H}_2\text{O}$ (99%, Riedel de Haen), phenazine (Sigma Aldrich), acridine (Sigma Aldrich), quinoline (98%, Sigma Aldrich), ethanol (EtOH) (99.5%, Merck) and methanol (MeOH) (99%, Merck).

All reactions followed a similar general synthetic procedure. To test the effect of stoichiometry on the obtained reaction products, three analogous reactions in each experiment, wherein the L:MX₂ ratios were varied from 2:1 to 1:1 to 1:2, were performed. Good quality single crystals were harvested from reaction vessels, with no attempt made to maximise the yields from crystallisation. Only the reaction procedures in which crystalline products suitable for analysis by SXRD were obtained are reported below. Matching of the experimental PXRD patterns with the PXRD patterns simulated from SXRD data, for all compounds, is given in the ESI.† Microanalyses of compounds, of which enough material could be obtained, were performed using a Flash 2000 CHNS-O analyzer fitted with an autosampler.

Synthesis of $[\text{Cd}(\mu\text{-Cl})_2(\text{acr})]_\infty$ (1). $\text{CdCl}_2\cdot 2.5\text{H}_2\text{O}$ (0.27 mmol, 0.0613 g) was dissolved in 2 ml of MeOH, and a few drops of distilled H_2O to aid dissolution. The solution was added to a stirred solution of acr (0.27 mmol, 0.0504 g) dissolved in 6 ml of MeOH. The resulting solution was left at room temperature (*ca.* 23 °C) open to the atmosphere to crystallise. A batch of light yellow, needle-like crystals of 1 was harvested upon formation. Found for 1: C, 43.07; H, 2.50; N, 3.86%; calcd. for $\text{C}_{13}\text{H}_9\text{NCdCl}_2$: C, 42.91; H, 2.30; N, 4.10%.

Synthesis of $[\text{Cd}(\mu\text{-Br})_2(\text{acr})]_\infty$ (2). A solution of $\text{CdBr}_2\cdot 4\text{H}_2\text{O}$ (0.14 mmol, 0.0319 g) dissolved in 2 ml of CH_3CN was added to a stirred solution of acr (0.30 mmol, 0.052 g) dissolved in

Table 7 Coordination geometries adopted by Cd²⁺ and Hg²⁺ cations with the increase in both bridging halide ligand size and width of the coordinated N-donor ligand

M ²⁺	μ-X	N-donor ligand		
		py	quin	acr
Cd ²⁺	Cl ⁻	Oh	Oh	TBP
	Br ⁻	Oh	TBP	TBP
	I ⁻	Td	Td	TBP
Hg ²⁺	Cl ⁻	Oh	TBP	TBP
	Br ⁻	Td	TBP	TBP
	I ⁻	Td	Td/pseudo-TBP	Td/pseudo-TBP

6 ml of MeOH. The resulting solution was left at room temperature (*ca.* 23 °C) open to the atmosphere to crystallise. A batch of brown-yellow, cubic crystals of **2** was harvested upon formation. Found for **2**: C, 34.59; H, 2.01; N, 3.10%; calcd. for C₁₃H₉NCdBr₂: C, 34.62; H, 2.10; N, 3.32%.

Synthesis of [Cd(μ-I)₂(acr)]_∞ (3). A solution of CdI₂ (0.30 mmol, 1.016 g) dissolved in 2 ml of MeOH was added to a stirred solution of acr (0.30 mmol, 0.0523 g) dissolved in 6 ml of MeOH. The resulting solution was left at room temperature (*ca.* 23 °C) open to the atmosphere to crystallise. A batch of dark brown-yellow, cubic crystals of **3** was harvested upon formation. Found for **3**: C, 28.97; H, 1.85; N, 2.80%; calcd. for C₁₃H₉NCdI₂: C, 28.63; H, 1.66; N, 2.57%.

Synthesis of [Hg(μ-Cl)₂(acr)]_∞ (4). A solution of HgCl₂ (0.30 mmol, 0.0757 g) dissolved in 2 ml of MeOH was added to a stirred solution of acr (0.30 mmol, 0.0517 g) dissolved in 6 ml of MeOH. The resulting solution was left at room temperature (*ca.* 23 °C) open to the atmosphere to crystallise. A batch of dark yellow, needle-like crystals of **4** was harvested upon formation.

Synthesis of [Hg(μ-Br)₂(acr)]_∞ (5). A solution of HgBr₂ (0.30 mmol, 0.1005 g) dissolved in 2 ml of THF was added to a stirred solution of acr (0.30 mmol, 0.0491 g) dissolved in 6 ml of THF. The resulting solution was left at room temperature (*ca.* 23 °C) open to the atmosphere to crystallise. A batch of yellow-brown, needle-like crystals of **5** was harvested upon formation.

Synthesis of [Hg₂(μ-I)₂I₂(acr)₂] (6). A solution of HgI₂ (0.30 mmol, 0.126 g) dissolved in 2 ml of MeOH was added to a stirred solution of acr (0.30 mmol, 0.0489 g) dissolved in 6 ml of MeOH. The resulting solution was left at room temperature (*ca.* 23 °C) open to the atmosphere to crystallise. A batch of orange-yellow, cubic crystals of **6** was harvested upon formation.

Synthesis of [Cd(μ-Cl)₂(phe)]_∞ (7). CdCl₂·2.5H₂O (0.27 mmol, 0.0634 g) was dissolved in 2 ml of MeOH, and a few drops of distilled H₂O to aid dissolution. The solution was added to a stirred solution of phe (0.27 mmol, 0.0498 g) dissolved in 6 ml of MeOH. The resulting solution was left at room temperature (*ca.* 23 °C) open to the atmosphere to crystallise. A batch of light yellow, needle-like crystals of **7** was harvested upon formation.

Synthesis of [Hg(μ-Cl)₂(phe)]_∞ (8). A solution of HgCl₂ (0.30 mmol, 0.0753 g) dissolved in 2 ml of CH₃CN was added to a stirred solution of phe (0.30 mmol, 0.0522 g) dissolved in 6 ml of CH₃CN. The resulting solution was left at room temperature (*ca.* 23 °C) open to the atmosphere to crystallise. A batch of yellow-brown, needle-like crystals of **8** was harvested upon formation.

Synthesis of [Hg(μ-Br)₂(phe)]_∞ (9). A solution of HgBr₂ (0.27 mmol, 0.1000 g) dissolved in 2 ml of MeOH was added to a stirred solution of phe (0.27 mmol, 0.0542 g) dissolved in 6 ml of MeOH. The resulting solution was left at room temperature (*ca.* 23 °C) open to the atmosphere to crystallise. A batch of yellow-brown, needle-like crystals of **9** was harvested upon formation.

Synthesis of [Hg₂(μ-phe)(μ-Br)₄] (10). A solution of HgBr₂ (0.55 mmol, 0.1900 g) dissolved in 2 ml of MeOH was added to a stirred solution of phe (0.27 mmol, 0.0514 g) dissolved in 6 ml of MeOH. The resulting solution was left at room temperature (*ca.* 23 °C) open to the atmosphere to crystallise. A batch of yellow-brown, needle-like crystals of **10** was harvested upon formation.

Synthesis of [Hg(μ-Cl)₂(quin)]_∞ (11). A solution of HgCl₂ (0.78 mmol, 0.1909 g) dissolved in 2 ml of EtOH was added to a slightly heated and stirred solution of quin (0.77 mmol, 0.0962 g) dissolved in 6 ml of EtOH. The resulting solution was left at room temperature (*ca.* 23 °C) open to the atmosphere to crystallise. A batch of colourless, needle-like crystals of **11** was harvested upon formation. Found for **11**: C, 27.34; H, 1.97; N, 3.71%; calcd. for C₉H₇NHgCl₂: C, 26.98; H, 1.76; N, 3.50%.

Synthesis of [Hg(μ-Br)₂(quin)]_∞ (12). A solution of HgBr₂ (0.78 mmol, 0.2801 g) dissolved in 2 ml of EtOH was added to a slightly heated and stirred solution of quin (0.77 mmol, 0.1097 g) dissolved in 6 ml of EtOH. The resulting solution was left at room temperature (*ca.* 23 °C) open to the atmosphere to crystallise. A batch of colourless, needle-like crystals of **12** was harvested upon formation. Found for **12**: C, 17.46; H, 1.26; N, 2.42%; calcd. for C₉H₇NHgBr₂: C, 22.08; H, 1.44; N, 2.86%.

Synthesis of [Hg₂(μ-I)₂I₂(quin)₂] (13). A heated solution of HgI₂ (0.78 mmol, 0.3507 g) dissolved in 2 ml of EtOH was added to a slightly heated and stirred solution of quin (0.77 mmol, 0.0978 g) dissolved in 6 ml of EtOH. The resulting solution was left at room temperature (*ca.* 23 °C) open to the atmosphere to crystallise. A batch of white, needle-like crystals of **13** was harvested upon formation.

Crystallographic studies

X-ray diffraction data for three of the thirteen reported structures, namely compounds **2**, **4** and **5**, were collected using a Bruker-Nonius Kappa CCD diffractometer at the X-ray Laboratory of the University of Cambridge, UK, at 180(2) K, employing φ and ω scans and MoK α radiation with a wavelength λ of 0.71073 Å obtained from a fine-focus sealed tube. The software packages Collect²⁹ and Sortav³⁰ were used to

Table 8 Intra- and intermolecular hydrogen bonding and contact parameters [\AA , $^\circ$] for compounds **1–13**

	Intramol. D–H \cdots A (\AA)	$d(\text{D–H})$ (\AA)	$d(\text{H}\cdots\text{A})$ (\AA)	$d(\text{D}\cdots\text{A})$ (\AA)	$\angle(\text{DHA})$ ($^\circ$)	Symmetry operator
1	C(2)–H(2) \cdots Cl(1) ^{#a}	0.93	2.89	3.792(8)	162.8	
2	C(2)–H(2) \cdots Br(1) ^{#a}	0.93	3.01	3.918(4)	166.4	
3	C(2)–H(2) \cdots I(1) ^{#a}	0.93	3.13	4.058(3)	173.6	
7	C(2)–H(2) \cdots Cl(1) ^{#b}	0.93	2.86	3.732(3)	156.3	#a $-x + 1, y, -z + 3/2$ #b $-x, y, 1/2 - z$
4	C(2)–H(2) \cdots Cl(1) ^{#a}	0.93	2.88	3.783(11)	164.8	
5	C(2)–H(2) \cdots Br(1) ^{#a}	0.93	2.96	3.875(4)	168.8	
8	C(6)–H(6) \cdots Cl(1) ^{#c}	0.93	2.98	3.532(8)	163.6	
	C(12)–H(12) \cdots Cl(2) ^{#d}	0.93	2.94	3.506(8)	121.1	
9	C(6)–H(6) \cdots Br(2) ^{#c}	0.93	3.02	3.610(8)	122.6	#c $-x, -y + 1, -z + 1$
	C(12)–H(12) \cdots Br(1) ^{#e}	0.93	2.90	3.808(11)	166.2	#d $-x + 1, -y + 1, -z + 1$ #e $x + 1, y, z$
10	C(2)–H(2) \cdots Br(2)	0.93	3.07	3.925(4)	154.0	
	C(5)–H(5) \cdots Br(1) ^{#c}	0.93	2.91	3.823(4)	169.0	
11	C(8)–H(8) \cdots Cl(2)	0.93	3.050	3.92(2)	156	
	C(1)–H(1) \cdots Cl(1) ^{#f}	0.93	3.124	3.77(2)	127	
12	C(8)–H(8) \cdots Br(2)	0.93	3.162	4.04(1)	157.6	
	C(1)–H(1) \cdots Br(1)	0.93	3.164	3.84(1)	131.5	
13	C(1)–H(1) \cdots I(2)	0.93	3.290	3.961(17)	130.9	#f $1 - x, 1 - y, 1 - z$
6	C(12)–H(12) \cdots I(1)	0.93	3.1464	3.869(5)	134.3	
	C(2)–H(2) \cdots I(1)	0.93	3.1095	4.010(5)	158.7	
	Intermol. D–H \cdots A (\AA)	$d(\text{D–H})$ (\AA)	$d(\text{H}\cdots\text{A})$ (\AA)	$d(\text{D}\cdots\text{A})$ (\AA)	$\angle(\text{DHA})$ ($^\circ$)	Symmetry operator
1	C(5)–H(5) \cdots Cl(1) ^{#b}	0.93	2.771	3.645(8)	157.0	#b $-x, y, 1/2 - z$
2	C(5)–H(5) \cdots Br(1) ^{#b}	0.93	2.91	3.800(4)	161.0	
3	C(5)–H(5) \cdots I(1) ^{#b}	0.93	3.08	3.990(2)	167.4	
7	C(5)–H(5) \cdots Cl(1) ^{#b}	0.93	2.84	3.742(3)	162.7	
4	C(5)–H(5) \cdots Cl(1) ^{#b}	0.93	2.85	3.63(1)	158.6	
5	C(5)–H(5) \cdots Br(1) ^{#b}	0.93	2.88	3.781(4)	163.2	
8	C(3)–H(3) \cdots Cl(1) ^{#g}	0.93	2.80	3.697(7)	119.6	#g $-x, -y, -z + 1$
	C(9)–H(9) \cdots Cl(2) ^{#h}	0.93	2.85	3.745(7)	162.2	
9	C(3)–H(3) \cdots Br(2) ^{#g}	0.93	2.94	3.834(11)	160.7	#h $-x + 1, -y, -z + 1$
	C(9)–H(9) \cdots Br(1) ^{#h}	0.93	3.08	3.654(8)	121.5	
11	C(2)–H(2) \cdots Cl(1) ^{#i}	0.93	2.83	3.69(2)	154.7	#i $x, y - 1, z$
12	C(2)–H(2) \cdots Br(1) ^{#j}	0.93	2.982	3.814(9)	149.7	#j $1 - x, 2 - y, 2 - z$
13	C(8)–H(8) \cdots I(1)	0.93	3.268	4.105(17)	150.9	
6	C(9)–H(9) \cdots I(2)	0.93	3.1222	4.021(6)	158.4	

carry out data reduction and absorption corrections. All other X-ray diffraction data were collected internally using a Bruker D8 Venture diffractometer, with a Photon 100 CMOS detector, at 293(2) K, employing a combination of φ and ω scans. Data collections were performed at 293(2) K to avoid temperature-dependent polymorphic transitions. Monochromatic MoK α radiation with a wavelength λ of 0.71073 \AA , from an I μ S source, was employed as the irradiation source. Data reduction and absorption corrections were performed using SAINT³¹ and SADABS³² as part of the APEX II suite.³³

Indexing and determination of the twinning matrix for structure **11** was conducted using CELL NOW.³⁴ The structures were solved by direct methods using SHELXS-97,³⁵ as part of the WinGX suite.³⁶ Structure refinements were carried out using SHELXL³⁵ in WinGX³⁶ as the GUI. Non-hydrogen atoms were refined anisotropically. Hydrogen atoms on aromatic ring carbon atoms were placed geometrically using a riding model, with a C–H distance of 0.930 \AA . Graphics and publication material were generated using ORTEP,³⁶ PLATON¹⁹ and Mercury 3.5 (ref. 18) (CCDC reference numbers 1409084–

Table 9 Aromatic ring interaction parameters in 1-13^a

	Cg(Z)–Cg(Z)	Cg–Cg (Å)	α (°)	β (°)	γ (°)	Cg(I) _p (Å)	Cg(J) _p (Å)	Slippage (Å)	Symmetry operator
1	Cg(N1)–Cg(N1) ^{#1}	3.715(3)	0	25.7	25.7	3.347(2)	3.347(2)	1.613	^{#1} $-x, 1 - y, 1 - z$
2	Cg(N1)–Cg(N1) ^{#1}	3.8985(18)	0	29.0	29.0	3.4110(12)	3.4110(12)	1.888	^{#2} $1 - x, -y, -z$
3	Cg(N1)–Cg(N1) ^{#1}	4.1986(12)	0	35.97	35.97	3.3979(8)	3.3979(8)	2.466	
7	Cg(N1)–Cg(N1) ^{#2}	3.7408(14)	0	25.7	25.7	3.3707(9)	3.3708(9)	1.622	
4	Cg(N1)–Cg(N1) ^{#1}	3.803(4)	0	27.33	27.33	3.379(3)	3.378(3)	1.746	
5	Cg(N1)–Cg(N1) ^{#1}	4.0039(3)	0	31.0	31.0	3.4323	3.4323	2.062	
8	Cg(N1)–Cg(N1) ^{#3}	3.810(4)	0	25.9	25.9	–3.428(3)	–3.428(3)	1.663	^{#3} $-x, -y, 1 - z$
	Cg(N1)–Cg(N1) ^{#4}	3.905(4)	0	24.9	24.9	3.543(3)	3.543(3)	1.643	^{#4} $1 - x, -y, 1 - z$
9	Cg(N1)–Cg(N1) ^{#3}	3.873(6)	0	28.8	28.8	–3.395(4)	–3.395(4)	1.864	^{#5} $-1 + x, y, z$
	Cg(N1)–Cg(N1) ^{#4}	4.059(6)	0	27.1	27.1	3.612(4)	3.613(4)	1.851	
10	Cg(N1)–Cg(N1) ^{#5}	4.082(2)	0	29.5	29.5	3.5545(14)	–3.5545(14)	2.008	
11	Cg(N1)–Cg(C8) ^{#6}	3.850(12)	1.2(10)	25.3	24.2	3.511(8)	3.479(9)		^{#6} $1 - x, 2 - y, -z$
	Cg(C8)–Cg(N1) ^{#7}	3.798(12)	1.2(10)	21.4	21.1	–3.542(9)	–3.536(8)		^{#7} $-x, 2 - y, -z$
12	Cg(C8)–Cg(N1) ^{#8}	3.985(5)	0.5(4)	25.6	25.1	3.610(4)	3.595(4)		^{#8} $1 - x, 1 - y, 1 - z$
	Cg(C8)–Cg(N1) ^{#9}	3.954(5)	0.5(4)	23.4	23.4	–3.628(4)	–3.630(4)		^{#9} $-x, 1 - y, 1 - z$
13	Cg(N1)–Cg(N1) ^{#10}	3.605(9)	0	16.0	16.0	–3.466(6)	–3.466(6)	0.991	^{#10} $-x, 1 - y, 1 - z$
	Cg(C4)–Cg(C4) ^{#11}	3.586(9)	0	11.8	11.8	3.510(6)	3.510(6)	0.733	^{#11} $-x, 2 - y, 1 - z$
	Cg(N1)–Cg(C4) ^{#10}	4.357(9)	0.5(7)	37.2	37.2	–3.469(6)	–3.457(6)		^{#12} $1 - x, -y, -z$
	Cg(C4)–Cg(N1) ^{#11}	4.419(9)	0.5(7)	37.2	37.2	3.504(6)	3.518(6)		^{#13} $1 - x, 1 - y, -z$
6	Cg(N1)–Cg(N1) ^{#12}	4.330(3)	0	37.1	37.1	–3.416(2)	–3.415(2)	2.614	
	Cg(N1)–Cg(N1) ^{#13}	4.843(3)	0	45.2	45.2	3.452(2)	3.452(2)	3.434	

^a Cg refers to the centroid of the six-membered heterocyclic ring with Cg–Cg being the distance between the ring centroids. α is the dihedral angle between planes *I* and *J*, β is the angle between the Cg(*I*)–Cg(*J*) vector and the normal to plane *I*, γ is the angle between the Cg(*I*)–Cg(*J*) vector and the normal to plane *J* (°). Cg(*I*)_p is the perpendicular distance of Cg(*I*) on ring *J* and Cg(*J*)_p is the perpendicular distance of Cg(*J*) on ring *I* (Å). Slippage is the distance between Cg(*I*) and the perpendicular projection of Cg(*J*) on ring *I* (Å).

1409096). Powder X-ray diffraction patterns were measured on a Bruker D2 Phaser powder diffractometer employing a Si low-background sample holder.

Acknowledgements

The authors would like to thank Peet van Rooyen and Dave Liles for assistance with crystallographic aspects. CS gratefully acknowledges the National Research Foundation for financial support through an Innovation Scholarship (SFH20100706000011827). MR acknowledges financial support from the University of Pretoria and the National Research Foundation (Grant No. 87659).

References

- C. B. Aakeröy, N. R. Champness and C. Janiak, *CrystEngComm*, 2010, **12**, 22.
- D. Braga, L. Brammer and N. R. Champness, *CrystEngComm*, 2005, **7**, 1.
- D. Braga, G. R. Desiraju, J. S. Miller, A. G. Orpen and S. L. Price, *CrystEngComm*, 2002, **4**, 500.
- G. R. Desiraju, *J. Chem. Sci.*, 2010, **122**, 667.
- D. Braga, *Chem. Commun.*, 2003, 2751.
- C. Hu, Q. Li and U. Englert, *CrystEngComm*, 2003, **5**, 519.
- R. Wang, C. W. Lehmann and U. Englert, *Acta Crystallogr., Sect. B: Struct. Sci.*, 2009, **65**, 600.
- C. Hu and U. Englert, *CrystEngComm*, 2001, **23**, 1.
- C. Hu, I. Kalf and U. Englert, *CrystEngComm*, 2007, **9**, 603.
- G. Mahmoudi and A. Morsali, *CrystEngComm*, 2009, **11**, 1868.
- C. Slabbert and M. Rademeyer, *Coord. Chem. Rev.*, 2015, **288**, 18.
- A. Morsali and M. Y. Masoomi, *Coord. Chem. Rev.*, 2009, **253**, 1882.
- U. Englert, *Coord. Chem. Rev.*, 2010, **254**, 537.
- G. A. Bowmaker, S. I. Rahajoe, B. W. Skelton and A. H. White, *Z. Anorg. Allg. Chem.*, 2011, **637**, 1361.
- F. R. Allen, *Acta Crystallogr., Sect. B: Struct. Sci.*, 2002, **58**, 380.
- D. Grdenić, *Q. Rev., Chem. Soc.*, 1964, **19**, 303.
- G. Meyer and P. Nockemann, *Z. Anorg. Allg. Chem.*, 2003, **629**, 1447.
- C. F. Macrae, P. R. Edgington, P. McCabe, E. Pidcock, G. P. Shields, R. Taylor, M. Towler and J. van de Streek, *J. Appl. Crystallogr.*, 2006, **39**, 453.
- A. L. Spek, *Acta Crystallogr., Sect. D: Biol. Crystallogr.*, 2009, **65**, 148.
- C. Janiak, *J. Chem. Soc., Dalton Trans.*, 2000, 3885–3896.
- H. R. Khavasi and A. A. Tehrani, *Inorg. Chem.*, 2013, **52**, 2891.
- J. R. Allan, A. D. Paton, A. J. Blake and K. Turvey, *Acta Crystallogr., Sect. C: Cryst. Struct. Commun.*, 1989, **45**, 1422.

- 23 G. G. Evans and J. C. A. Boeyens, *Acta Crystallogr., Sect. B: Struct. Sci.*, 1989, **45**, 581.
- 24 K. Lamberts, I. Kalf, A. Ramadan, P. Müller, R. Dronskowski and U. Englert, *Polymer*, 2011, **3**, 1151.
- 25 H. W. Roesky and M. Andruh, *Coord. Chem. Rev.*, 2003, **236**, 91.
- 26 A. J. Canty, C. L. Raston, B. W. Skelton and A. H. White, *J. Chem. Soc., Dalton Trans.*, 1982, 15.
- 27 H. Mohd, A. S. Puvaneswary, W. J. Basirun and S. W. Ng, *Main Group Met. Chem.*, 2005, **28**, 171.
- 28 D. Venkataraman, Y. Du, S. R. Wilson, K. A. Hirsch, P. Zhang and J. S. Moore, *J. Chem. Educ.*, 1997, **74**, 915.
- 29 R. W. W. Hooft, *COLLECT*, Nonius BV, Delft, The Netherlands, 1988.
- 30 R. H. Blessing, *Acta Crystallogr., Sect. A: Found. Crystallogr.*, 1995, **51**, 33.
- 31 Bruker, *SAINT+*, Bruker AXS Inc., Madison, Wisconsin, USA, 2007.
- 32 G. M. Sheldrick, *SADABS*, University of Göttingen, Germany, 1996.
- 33 Bruker, *APEX II*, Bruker AXS Inc., Madison, Wisconsin, USA, 2013.
- 34 G. Sheldrick, *CELL NOW*, University of Göttingen, Germany, 2005.
- 35 G. M. Sheldrick, *Acta Crystallogr., Sect. A: Found. Crystallogr.*, 2008, **64**, 112.
- 36 L. J. Farrugia, *J. Appl. Crystallogr.*, 2012, **45**, 849.